

Predictive capabilities of the integrated modeling TRANSP code for tokamak plasmas

A.Y. Pankin¹, J. Breslau¹, M.V. Gorelenkova¹, R. Budny¹, M. Goliyad², B.A. Grierson³,
G.W. Hammett¹, S.C. Jardin¹, J.B. Lestz^{3,4}, and X. Yuan⁵

¹Princeton Plasma Physics Laboratory, Princeton, NJ 08540

²Rutgers University, Piscataway, NJ 08854

³General Atomics, San Diego, CA 92121

⁴University of California, Irvine, CA 92697

⁵Argonne National Laboratory, Lemont, IL 60439

Abstract

This paper expands on the TRANSP description given in *Computer Physics Communications* 312 (2025) 109611 by describing recent progress in TRANSP's predictive functionality and emphasizing development of the PT_SOLVER module and integration of the high-fidelity T3D/GX framework for plasma profile prediction using a high-fidelity gyrokinetic model for turbulent transport. PT_SOLVER is a modular, multi-region, parallel solver for coupled transport equations of particle density, electron and ion energy, and toroidal angular momentum that uses an implicit Newton method to advance the solution of these equations. The numerical formulation includes source coupling, moving-geometry terms, and nonlinear stabilization based on modified Péclet numbers, thereby enabling the PT_SOLVER to handle the stiffness associated with gradient-dependent transport models. Stabilization occurs via a nonlinear function controlling discretization in zones of steep gradients or rapidly changing transport coefficients. Source terms that account for heating, current drive, alpha-particle effects, and collisional energy exchange are handled thoroughly, and both residual norms and profile-change measures are used to assess convergence. Verification is carried out using analytical benchmark solutions, manufactured solution benchmarks, convergence studies of stiff gradient-dependent diffusivities, and code-to-code comparisons of TGYRO using the TGLF/NEO models for anomalous and neo-classical transport. A multi-level parallel decomposition strategy in PT_SOLVER is described for both flux surface and TGLF wavenumber parallelism, along with representative scaling results. This paper also describes the TRANSP Interface to the modular T3D/GX workflow and presents verification examples related to the interface for coupled prediction simulations. Agreement between PT_SOLVER and the modular T3D solver is confirmed by a benchmark set under rising complexity in physics. The results in this paper confirm that the predictive TRANSP framework has a robust numerical implementation for time-dependent predictive transport simulations, and it provides a basis for future hybrid reduced and high-fidelity workflows.

1 Introduction

The development of controlled thermonuclear fusion offers a pathway to clean and sustainable energy. Tokamaks are among the most promising magnetic confinement devices, and the TRANSP

integrated modeling code [1–3] has long served as a critical tool for both interpretive and predictive analysis of tokamak plasmas. For predictive analysis, the code is actively used for model verification and validation, plasma scenario planning and assessments of future tokamak devices [4–12].

Integrated predictive modeling plays an important role in tokamak fusion research. It is essential for optimizing experiments, developing scenarios, and determining how a new regime will operate. Predictive modeling can provide a series of evolving plasma profiles in time consistent with realistic sources of heating, particles, and momentum; transport of particles and energy; and plasma equilibrium. Interpretive analysis results are being used to create databases of plasma discharges. Predictive simulations are used to evaluate the effects of changing the heating, fueling, current drive, rotation, impurity level or control paths *prior* to performing an experiment. They are used for designing future tokamaks such as ITER. The simulation will only be valid if the underlying physics-based transport models used for the computations have a high level of physics fidelity and a robust numerical implementation.

TRANSP’s long history as a leading integrated modeling tool for tokamak analysis stems from its use in interpretive analyses of the experimental data through the combination of data from experimental measurements, equilibrium reconstructions, and source calculations, which are combined to infer transport and power balance. The code can also provide predictive capability and time evolution of plasma profiles through the same integrated framework using theory-based transport models and consistent treatments of heating, current drive, particle, and momentum sources. The close connection between interpretive and predictive functions in TRANSP is one of its key strengths, as both rely on the same infrastructure to provide geometries, evaluate sources, and couple physics. This establishes the direct applicability of predictive calculations to experimental analyses and validations of models.

TRANSP simulates the time-dependent evolution of plasma profiles, including density, temperature, and toroidal rotation, by integrating coupled conservation equations that account for heating, current drive, and complex equilibrium effects. In this paper, “predictive” TRANSP refers specifically to simulations in which the time evolution of kinetic profiles, such as temperature, density, and toroidal rotation, is advanced using transport equations and theory-based models for anomalous and neoclassical transport. This is distinct from other time-dependent TRANSP capabilities, such as current-diffusion workflows, which may also evolve plasma quantities in time but are not the focus of the present work.

Other integrated modeling workflows commonly used for transport prediction include AS-TRA [13], JETTO [14], JINTRAC [15], and IPS-FASTRAN [16, 17]. These tools address related predictive-transport problems, but they differ from TRANSP/PT_SOLVER in workflow organization, coupling strategy, and the degree to which source, equilibrium, and transport physics are embedded within a single established TRANSP framework. Recent workflows relevant to predictive transport also include FUSE [18], which supports integrated steady-state and time-dependent plasma modeling in a broader fusion-design framework, and TORAX [19], a fast differentiable core transport simulator implemented in JAX.

A key module within predictive TRANSP is PT_SOLVER, which integrates the nonlinear transport equations using an implicit, Newton-based iterative method. Convergence is monitored by a normalized residual, combined with maximum relative change and maximum pointwise residual criteria.

A detailed overview of the capabilities of the code, including the general predictive process and the options available for prediction, has recently been presented in Ref. [3]. Therefore, the purpose of this article is not to duplicate this overview, but to deal with one of the important elements of the code that was not described with sufficient algorithmic detail there.

Three important features of PT_SOLVER are worth mentioning here. First, PT_SOLVER uses

a multi-region approach whereby different anomalous and neoclassical transport models may be used in different radial regions, such as axial, confinement, and edge regions. This provides useful flexibility in cases where a single transport model may not be sufficient to describe the physics throughout the whole radius of the plasma – for example, when an anomalous or neoclassical model is not valid in a particular plasma region. In particular, it might not be valid near the magnetic axis or in the plasma edge. The original reference TRANSP paper [3] includes the description of how the transport models can be combined for different confinement regions. Second, PT_SOLVER was designed for multilevel parallelization to ensure that both the transport advance and the computational expense of evaluating the transport models could be distributed using modern computing architectures. Specifically, the implementation of the anomalous transport TGLF model in PT_SOLVER includes parallelism over the flux surfaces combined with parallelism over the TGLF wavenumbers, thus eliminating the constraint wherein the number of processors would have to equal the number of transport zones. Lastly, PT_SOLVER is engineered to address the stiffness associated with the gradient sensitivity of transport closures in a turbulence model by implementing an implicit Newton-based nonlinear solver enhanced with stabilization techniques based on the modified Péclet number.

Previous work by Jardin *et al.* [20] identified the numerical difficulties related to the use of gradient-dependent transport coefficients, emphasized the need to develop robust stabilization techniques, and provided an outline of a numerical scheme to address these difficulties. The code’s current implementation of the predictive process in PT_SOLVER differs from this numerical scheme, and there is no documented reference on the current PT_SOLVER numerical algorithm. Indeed, the implicit multi-channel method used by TRANSP has specific features related to source treatment, moving geometry, Péclet number stabilization, and nonlinear convergence tests. Therefore, a detailed description of the code’s predictive process is provided as a reference for users of the code and as a basis for code-to-code verification of the predictive solver. This description should assist in clearly identifying both the capabilities and current limitations associated with predictive transport simulations performed with TRANSP.

The primary motivation for focusing on this area is due to the computational intensity of predictive transport simulations in tokamaks, even though their established transport models are considered relatively mature. The equations governing transport are highly nonlinear, tightly coupled over multiple transport channels, and will be sensitive to geometry, boundary conditions, collisional interactions, auxiliary heating, particle sources, and momentum input. Additionally, several transport closures used in predictive studies generally yield diffusion and pinch coefficients that depend greatly on local gradients and also can change drastically over space and time. Therefore, in this environment, it is very difficult to use explicit approaches or naive implicit discretizations, which often lead to imprecise, oscillatory, and/or unstable solutions. Thus, a successful predictive working process requires an appropriate transport model and a transport solver that provides stable, modular, and reliable convergence behavior across a wide range of plasma operation conditions.

PT_SOLVER is the component in TRANSP designed to address these requirements. PT_SOLVER provides a multi-channel, implicit transport solution for predicting how the temperatures of electrons and ions, plasma density, composition of impurities, and toroidally rotating plasma evolve over time using the standard TRANSP flux-surface average framework. PT_SOLVER includes a selection of anomalous and neoclassical transport models that are coupled to the rest of TRANSP’s integrated modeling workflow. Since PT_SOLVER shares the same TRANSP framework that is used for calculations of equilibrium and sources, it is internally self-consistent and can be applied for full-device predictive simulations. For this reason, in order to provide confidence in the interpretation of predicted results from TRANSP, it is essential to have a clearly defined numerical description, along with an appropriate verification strategy for PT_SOLVER.

The verification method employed in this paper focuses on the verification of PT_SOLVER itself, not the models for anomalous and neoclassical transport that it can use. We do not compare the results with experiment, but only with the predictions of other solvers that utilize the same theory-based model for anomalous transport. The objective here is to verify that the prediction from PT_SOLVER yields the same profiles as those predicted by a different solver, given the same inputs. The focus of this verification exercise is the coupling or numerical implementation. This type of comparison also serves as a complement to internal testing against simplified cases and provides a higher quality of information than simply looking at profile comparisons for the two cases.

Another aspect related to the solver-centric focus of the TRANSP code is its recent extension to allow more modular approaches to transport and turbulence workflows, such as coupling to T3D [21, 22] and the nonlinear gyrokinetic GX model [23, 24]. This is significant because it supports the development of predictive calculations by coupling profile evolutions to higher-fidelity turbulence models, including GPU-based nonlinear gyrokinetic calculations. However, the goal of the present paper is not to provide a comprehensive verification and performance assessment of the coupling of the TRANSP/T3D/GX workflow, but rather to give an overview of the architecture of the coupling, show stable operation in an integrated environment, and to provide examples of how the predictive TRANSP framework can be connected to external transport and turbulence components.

The core contributions of this work are as follows. First, we present a comprehensive overview of the PT_SOLVER formulation used for predictive TRANSP simulations, providing detailed descriptions of the transport equations, discretization methods, nonlinear solution strategies, stabilization methods, and convergence criteria. Second, we describe the verification efforts for PT_SOLVER using a series of benchmark cases with the TGYRO code. Finally, we give an overview of the recent integration development between TRANSP, T3D, and GX that illustrates a modular approach to the extension of the predictive framework. By providing detailed information on the current development of predictive workflows, we have provided a primary methodological and verification contribution relating specifically to the predictive transport functionality of the TRANSP framework.

The 2025 TRANSP technical reference paper [3] provided general organization of the TRANSP predictive workflow, a summary of the capability of the TRANSP predictive code, and an overview of the transport modeling and predictive tools available for TRANSP. The emphasis of this paper is to present three specific contributions related to the PT_SOLVER numerical formulation. The first contribution is a detailed description of this formulation, including the discretization method used by PT_SOLVER, the use of coupling of the source terms, the method of handling moving geometry, the method of stabilizing nonlinearity using an adjusted Péclet number criterion, and the criteria that are used for convergence of iterative solutions in practical applications of the solver. The second contribution is to present a comprehensive hierarchy of verification tests for the predictive portion of the TRANSP code. This hierarchy includes analytically solved and manufactured solution verification tests, convergence tests for stiff gradient-dependent transport coefficients, and a code-to-code verification for PT_SOLVER and TGYRO using TGLF and NEO models for anomalous and neoclassical transport. The third contribution is to document key implementation features that were not discussed in detail in the above-referenced papers. These features include the multilevel parallelization method used in PT_SOLVER calculations for transport resolution and the initial modular coupling of the TRANSP to the T3D/GX predictive calculations. In this sense, the present paper is intended as a methodological and verification-focused supplement to the broader TRANSP capabilities paper, rather than as a second general review of predictive functionality.

This paper is structured as follows: Section 2 includes background and motivation. Section 3 describes the governing transport equations, predictive transport framework, and assumptions made

in the flux surface averaged formulation. In Section 4, we introduce the PT_SOLVER numerical algorithm, which incorporates the implicit Newton formulation, coefficient construction, stabilization procedure, and convergence metrics. It also includes additional cross-verification studies between PT_SOLVER and TGYRO. Section 5 discusses the integration path with T3D/GX and provides a first demonstration of the coupled workflow. Finally, Section 6 summarizes the current capabilities, limitations, and future direction of this work.

2 Background and motivation

Predictive transport simulations are an essential part of the integrated modeling process for a tokamak. The ability to calculate how the plasma profiles evolve over time self-consistently under the influence of prescribed sources, sinks and boundary conditions is a critical part of scenario development, experiment planning, actuator optimization, and extrapolation to future devices. In practical integrated modeling, this problem is typically formulated as a coupled set of one-dimensional transport equations written on magnetic flux surfaces and coupled to the time evolution of the equilibrium, heating and current drive, particle fueling, momentum input, and models for large-scale MHD events, such as sawtooth crashes. The importance of the overall integrated modeling context has been acknowledged for many years. The dynamic modeling of tokamak transport together with plasma position and control has been demonstrated previously [25] and described in detail in the literature [26]. These publications provide the numerical framework required for the predictive simulation of plasma in a toroidal geometry. Within this category of modeling integration tools, TRANSP has become a full-featured system used for both interpretive and predictive analyses of tokamak plasmas [3].

A significant issue for predictive simulation of transport processes is that physics processes create a stiffness that affects the numerical stability of transport solvers. In many applications, the nonlinear dependence of thermal and particle diffusivities, as well as the convective term, on local gradient values leads to potential difficulties with convergence, noise, and unintended numerical instability of simple implicit discretizations. Using an explicit approach, it has been demonstrated that gradient-dependent diffusion coefficients can produce severe numerical pathologies in one-dimensional diffusion situations [20]. Another approach to address the numerical stability has been proposed by Pereverzev and Corrigan [27]. The approach that they developed allows for significantly larger time steps compared to standard treatment and avoids artificial oscillations. These studies highlight the increasingly important role that numerical robustness and stability play in predictive transport modeling by demonstrating that they are not simply details of the implementation of the model, but actually represent a key element of the entire modeling effort.

To solve stiff transport equations, there are multiple possible algorithmic approaches. An efficient solver using the fourth-order interpolated differential operator (IDO) discretization with a method for nonlinear iteration that derives from a root-finding procedure has been recently developed [16]. Using this method, both a plasma transport variable and its gradient are advanced, yielding more spatial accuracy on relatively coarse radial grids. Recently, Ludvig-Osipov *et al.* developed formulations for the transport equations in conservative form using fourth-order IDO discretization combined with second-order implicit Runge-Kutta time-stepping and under-relaxed Picard iteration [28]. They focus on conservative properties, accuracy in transient periods, and robust convergence of solutions to stiff nonlinear transport models. These developments are examples of solver designs that employ higher-order discretizations combined with carefully chosen nonlinear iteration techniques to enhance accuracy and stability, while minimizing computation costs.

A somewhat different approach has been used for rapid predictive simulations for control, sce-

nario optimization, and repeated model evaluation with the RAPTOR code. Originally developed as a simulator for control, RAPTOR [29] generalized its application by providing the ability to simultaneously evolve the electron and ion densities and temperatures by using so called “first-principles-based surrogate codes” for rapid predictive simulations. Most of these applications have involved quick predictions of the performance of a set of parameters. Another enhancement to the code came with the implementation of the QLKNN model [30] for rapid optimization of stationary tokamak plasmas. In the case of the development of RAPTOR for tokamak operation using this new modeling system, the major objective was not to produce a fully integrated framework that utilizes both source and event physics, but rather to produce a workflow capable of efficiently making predictive assessments of data or models and assisting researchers to produce solutions more quickly than traditional approaches.

For higher levels of fidelity in physics, transport solvers have been directly coupled to gyrokinetic calculations. TGYRO [31] was developed for predicting steady-state profiles through direct gyrokinetic and neoclassical simulations. Another transport solver, TRINITY, supports time-dependent evolution of plasma profiles with turbulent fluxes computed with local nonlinear gyrokinetic turbulence simulations [32]. These efforts have provided important benchmarks for modern predictive workflows and have drawn a useful distinction between steady-state and time-dependent transport solvers. They have also demonstrated how coupling to advanced transport models creates additional constraints on solver stability, nonlinear convergence, and the management of computational costs.

The goal of PT_SOLVER is not just a high-fidelity gyrokinetic stand-alone transport solution, nor a real-time control application. Rather, PT_SOLVER is intended to be an embedded, practical, robust, and implicit multi-channel transport solver within the integrated TRANSP environment, where the profile predictions are consistent with the models for sources, equilibrium computations, and current drive physics. Within the TRANSP framework, PT_SOLVER has a clear path for validation against experiments due to the availability of the interpretive analysis within the same framework and multiple synthetic diagnostics, which make direct comparison with experiments straightforward. This objective sets the PT_SOLVER requirements as robustness, modularity, and integration with other physics models in TRANSP.

As described in 2025 reference paper [3], PT_SOLVER supports several anomalous transport models, including GLF23 [33, 34], TGLF [35, 36], MMM [37, 38], MM (Multi Mode model) [37, 38], RLW (Rebut-Lallia-Watkins model) [39], COPPI (Coppi-Tang model) [40], CDBM (Current Diffusive Ballooning Mode Model) [41, 42], USER, and Paleo (Paleoclassical) [43] models, together with neoclassical models such as the modified Chang-Hinton model [44], NEO [45, 46], and NCLASS [47]. From the time of the TRANSP reference publication, TGLF has been extended to use saturation rule3 (SAT3) [48] and surrogates for TGLF (TGLF-NN) [49] and GKNN [50] have been implemented in PT_SOLVER. Among anomalous models available in TRANSP, TGLF is particularly important in the present work because it provides a reduced, theory-based model of gyrokinetic turbulent transport while remaining practical enough for iterative predictive calculations. Its computational cost and evaluation over multiple flux surfaces motivate the multilevel parallelization strategy described below.

This paper describes the numerical scheme used for TRANSP predictive modeling. It does not attempt to present a comprehensive overview of all aspects of predictive workflows. Instead, it focuses on defining the PT_SOLVER equations and the implicit Newton-based solution strategy to solve them; describing how coupled transport channels, source terms and stabilization methods are treated in TRANSP; and defining criteria for convergence in predictive simulations. The verification of the solver is an important aspect of this work. The code-to-code comparisons using a common anomalous transport model, such as TGLF model [51], are especially valuable. They provide a

direct test of solver behavior rather than comparisons in which both the transport physics and the numerical framework differ simultaneously. This approach is also consistent with recent cross-verification and validation studies emphasizing the need to distinguish numerical agreement from broader model-validation questions [8].

In summary, there are three generic types of predictive transport approaches. The first one can be characterized as dynamic integrated modeling from a wider tokamak system perspective [25, 26]. The second group of applications focuses on developing a robust numerical method for time-stable solutions to stiff, nonlinear transport equations using unique discretization and iterative approaches for these equations [16, 20, 27, 28]. The third group focuses on either real-time, rapid control-oriented predictive simulations [29, 30], or directly coupling algorithms to gyrokinetic turbulence simulations [31, 32]. PT_SOLVER belongs most naturally to the first two classes. Its distinguishing role is to provide a robust, implicit, multi-channel transport capability inside TRANSP, with sufficient numerical stability to support predictive calculations using stiff transport closures in a mature integrated modeling environment.

3 Governing Transport Equations and Assumptions

The formulation assumes quasi-neutrality, with impurities in local thermodynamic equilibrium (LTE) using prescribed fractional abundances. Charge neutrality and effective charge (Z_{eff}) constraints relate electron, ion, and impurity densities. The evolution of flux surfaces (via $\partial\xi/\partial t$) is provided by an equilibrium solver, and geometric metric factors are retained in the discretization.

In a flux-surface – averaged coordinate ξ (normalized so that $\xi \in [0, 1]$), the general conservation law for a plasma variable $U(\xi, t)$ is

$$\frac{\partial U}{\partial t} + \frac{1}{V'} \frac{\partial}{\partial \xi} \left\{ V' \mathfrak{F}(U) \right\} = S(U), \quad (1)$$

where $V'(\xi) = \frac{dV}{d\xi}$ is the differential volume (or area) element, $\mathfrak{F}(U)$ represents the total flux (including diffusive, convective, and grid-motion contributions), and $S(U)$ includes all source and sink terms.

The following equations give the schematic channel structure; the discrete implementation retains the full TRANSP flux-surface geometry, density weighting, source coupling, and moving-grid terms described in Sec. 4. In particular, the particle density $n(\xi, t)$ satisfies

$$\frac{\partial n}{\partial t} + \frac{1}{V'} \frac{\partial}{\partial \xi} \left\{ V' \left[-D_n \frac{\partial n}{\partial \xi} + V_n n \right] - n \frac{\partial \xi}{\partial t} \right\} = S_n, \quad (2)$$

where D_n is the diffusivity, V_n is the convective (pinch) velocity, and S_n describes sources such as recycling, neutral beam injection, and fusion reactions. PT_SOLVER has separate options to advance densities for electrons, hydrogenic ions, and impurities.

For electrons, the energy conservation equation is

$$\frac{\partial(n_e T_e)}{\partial t} + \frac{1}{V'} \frac{\partial}{\partial \xi} \left\{ V' \left[-\chi_e \frac{\partial T_e}{\partial \xi} + V_{T_e} n_e T_e \right] - n_e T_e \frac{\partial \xi}{\partial t} \right\} = S_{T_e}, \quad (3)$$

and for ions,

$$\frac{\partial(n_i T_i)}{\partial t} + \frac{1}{V'} \frac{\partial}{\partial \xi} \left\{ V' \left[-\chi_i \frac{\partial T_i}{\partial \xi} + V_{T_i} n_i T_i \right] - n_i T_i \frac{\partial \xi}{\partial t} \right\} = S_{T_i}. \quad (4)$$

Here, $\chi_{e,i}$ denotes the effective thermal conductivities and $V_{T_{e,i}}$ the convective velocities. The source terms include collisional energy exchange: $Q_{ei} = n_e \nu_{ei} (T_e - T_i)$, where ν_{ei} is the electron-ion

collision frequency; recycling contribution Pe_{rcy} describing energy deposited by recycled neutrals; alpha particle heating Pe_α ; and other external sources, such as RF, neutral beam heating and radiative losses.

The toroidal angular momentum channel may be written schematically as

$$\frac{\partial p_\phi}{\partial t} + \frac{1}{V'} \frac{\partial}{\partial \xi} \left\{ V' \left[-\chi_\phi \frac{\partial \Omega_\phi}{\partial \xi} + V_\phi p_\phi \right] - p_\phi \frac{\partial \xi}{\partial t} \right\} = S_\phi, \quad (5)$$

where p_ϕ denotes the flux-surface-averaged toroidal angular momentum density, Ω_ϕ is the toroidal angular velocity, χ_ϕ is the momentum diffusivity, V_ϕ is the convective momentum pinch, and S_ϕ represents external torques and momentum sinks.

4 PT_SOLVER

This section outlines the PT_SOLVER numerical algorithm that is used to solve the transport equations that are described in the previous section. While the continuum formulation represents the essential physical content of the predictive problem, actual TRANSP simulations are dependent on the specific discretization that is contained within the code, including the implicit time-stepping scheme, linearization of transport operators, management of coupled sources and exchange terms, moving geometry effects, as well as the required nonlinear stabilization that is necessary for gradient-dependent transport coefficients. These terms are all significant because the PT_SOLVER algorithm is not simply another implementation of a previously developed algorithm for gradient-dependent diffusion problems. The PT_SOLVER algorithm is a code-specific implementation that is intended to solve robust multi-channel predictive problems within the TRANSP framework. As such, this section is intended to outline the discretized equations that are solved by PT_SOLVER as well as the resultant convergence criteria that are used to solve the nonlinear problem.

In addition to the mathematical description below, PT_SOLVER possesses certain other aspects of its design that are important from an engineering point of view. PT_SOLVER is a modular, parallel, multi-regional transport solver that communicates with the rest of TRANSP through the Plasma State interface. It accommodates three radial regions with possibly different models being used in each region: axial region, confinement region, and edge region. The usefulness of this approach lies not only in making coding easier but also in allowing predictive calculations to stay valid even if a particular model is relevant only to one part of the plasma. Further, it offers a controlled way to include different models for different radial positions in a global calculation. This capability becomes especially important when considering situations in which the turbulence model underpredicts transport coefficients in the core or physics of the pedestal and near-axis requires different assumptions than those suitable for the confinement region. The boundary conditions when the multi-region approach is enabled are described in Table 1.

PT_SOLVER has a two-level parallel capability for selected models. In particular, the TGLF model implementation in PT_SOLVER has one level of parallel processing for the transport solve for the individual flux surfaces, whereas another level can be used by TGLF, which has its own parallelism based on wavenumber decomposition. This approach utilizes sub-communicators for transport model calculations. After the TGLF computations are done, the information is combined by the solver for the Newton iteration process. There is more flexibility in terms of the number of processors available compared to approaches based only on the number of transport zones.

The main numerical challenge faced in predictive transport arises from the stiffness inherent to turbulence closures. Even in cases where the transport equation is not solved in terms of a threshold-based approach, there can be stiff behavior due to the strong dependence of the diffusivities and

Table 1: Summary of PT_SOLVER region definitions and boundary treatment in predictive TRANSP simulations. The notation $X_{\Upsilon, \text{bound}}$ denotes the outer predictive boundary for channel Υ , with $X_{T, \text{bound}} \equiv XIBOUND$ for temperature channels, $X_{n, \text{bound}} \equiv XNBOUND$ for density channels, and $X_{\phi, \text{bound}} \equiv XPHIBOUND$ for toroidal rotation.

Element	Radial extent	Role in predictive calculation	Boundary treatment / typical control
Inner boundary	$\xi = 0$	Magnetic-axis boundary for all evolved channels	Zero-gradient (Neumann-type) condition for evolved profiles
Axial region	$0 \leq \xi < XIMIN_CONF$	Optional region used when alternate transport assumptions are needed near the magnetic axis, e.g., where a confinement-region model is not reliable	Shares the inner boundary at $\xi = 0$ and couples continuously to the confinement region at $\xi = XIMIN_CONF$
Confinement region	$XIMIN_CONF \leq \xi \leq X_{\Upsilon, \text{bound}}$	Main predictive domain in which theory-based anomalous and neo-classical transport models are typically applied	Outer boundary for each channel is imposed at $X_{\Upsilon, \text{bound}}$ using prescribed edge data, fixed values, or pedestal-model output
Edge region	$X_{\Upsilon, \text{bound}} < \xi \leq 1$	Optional region used to represent the near-edge / pedestal domain with separate transport assumptions or prescribed profiles	Provides matching between the predictive solution and imposed edge constraints

pinches on evolving local gradients. In addressing this problem, PT_SOLVER uses a time-stepping algorithm based on the Newton method that is augmented with nonlinear stability conditions involving modified Péclet numbers, and with convergence conditions that consider both residuals and profile changes. The simpler problems of gradient-dependent diffusivities used in this paper do not constitute a replacement for the full TGLF framework, but serve merely as examples illustrating how stiffness can arise from transport parameters that depend strongly on evolving profiles.

4.1 Numerical Algorithm

PT_SOLVER uses an implicit time-advance combined with a Newton-based iterative method [20].

Assume the domain in ξ is discretized at grid points ξ_j with spacing $\Delta\xi$. A generic transport equation for a plasma variable is discretized via the following equation:

$$\frac{U_j^{n+1} - U_j^n}{\Delta t} + \mathfrak{L}_j^{n+1} = S_j, \quad (6)$$

with the time-discrete algebraic transport operator at time $n + 1$ approximated by

$$L_j^{n+1} = \frac{1}{\Delta t} \left(A_j U_{j-1}^{n+1} + B_j U_j^{n+1} + C_j U_{j+1}^{n+1} \right), \quad (7)$$

where A_j , B_j , and C_j are dimensionless coefficients after the finite-volume and time-step scaling.

Separating implicit terms on the left-hand side and explicit terms on the right-hand side yields

$$U_j^{n+1} + \mathfrak{L}_j^{n+1} \Delta t = -D_j \quad \text{with} \quad D_j = -U_j^n - S_j \Delta t. \quad (8)$$

Here, D_j includes a combination of known terms at the previous timestep n and the explicitly known source terms S_j . The coefficients A_j , B_j , C_j , and D_j are derived from the discretization of the diffusive and convective fluxes and depend on local transport coefficients and geometric factors. For the electron temperature equation, they take on the following form:

$$A_j = -\frac{\Delta t}{1.5 n_{e,j} V_j} \left[\hat{\chi}_{e,j-\frac{1}{2}} \frac{S_{j-\frac{1}{2}} n_{e,j-\frac{1}{2}}}{\Delta_{j-\frac{1}{2}}^r} F(\hat{P}_{e,j-\frac{1}{2}}) \right] + \frac{\Delta t \dot{\xi}}{2 n_{e,j} V_j} \xi_j n_{e,j} V_j', \quad (9)$$

$$B_j = 1 + \frac{\Delta t q_{ie,j}}{1.5 n_{e,j} V_j k_B} + \frac{V_j - V_j^{(n)}}{1.5 V_j} + \frac{\Delta t}{1.5 n_{e,j} V_j} \left[\hat{\chi}_{e,j+\frac{1}{2}} \frac{S_{j+\frac{1}{2}} n_{e,j+\frac{1}{2}}}{\Delta_{j+\frac{1}{2}}^r} \left(\hat{P}_{e,j+\frac{1}{2}} + F(\hat{P}_{e,j+\frac{1}{2}}) \right) \right. \\ \left. + \hat{\chi}_{e,j-\frac{1}{2}} \frac{S_{j-\frac{1}{2}} n_{e,j-\frac{1}{2}}}{\Delta_{j-\frac{1}{2}}^r} F(\hat{P}_{e,j-\frac{1}{2}}) \right] - \frac{\Delta t \dot{\xi}}{2 n_{e,j} V_j} [\xi_{j+1} n_{e,j+1} V_{j+1}' - \xi_j n_{e,j} V_j'], \quad (10)$$

$$C_j = -\frac{\Delta t}{1.5 n_{e,j} V_j} \left[\hat{\chi}_{e,j+\frac{1}{2}} \frac{S_{j+\frac{1}{2}} n_{e,j+\frac{1}{2}}}{\Delta_{j+\frac{1}{2}}^r} F(\hat{P}_{e,j+\frac{1}{2}}) \right] - \frac{\Delta t \dot{\xi}}{2 n_{e,j} V_j} \xi_{j+1} n_{e,j+1} V_{j+1}', \quad (11)$$

$$D_j = \frac{\Delta t Q_{e,j}}{1.5 n_{e,j} k_B V_j} + \frac{\Delta t \dot{\xi}}{2 V_j} n_{e,j} T_{e,j} (\xi_{j+1} V_{j+1}' - \xi_j V_j') + \frac{n_{e,j} T_{e,j} V_j}{\hat{n}_{e,j} \hat{V}_j}, \quad (12)$$

where T_j and $n_{e,j}$ are the electron temperature and electron density at j zone boundary at the previous time step, $n_{e,j}$ is the electron density at the current time step, ξ_j is the radial grid coordinate at j zone boundary, $\chi_{e,j+1/2}$ is the electron thermal diffusivity for j zone center, $S_{j\pm 1/2}$ is the surface area at j zone center, V_j is the zone volume, $V_j' = (\partial V / \partial \xi)|_j$ is the radial derivative of volume at j zone boundary, $\hat{P}_{e,j}$ is the modified electron Péclet number (which is discussed below), $q_{ie,j}$ is the electron-ion energy exchange rate at j zone boundary, $Q_{e,j}$ is the electron heating power density at spatial location j , k_B is the Boltzmann constant, $\dot{\xi} = \partial \xi / \partial t$ is term responsible for the grid radial motion, and Δ^r is the grid spacing defined as $d\xi / \langle |\nabla \xi| \rangle$. In the coupled T_e/T_i solve, the electron-ion exchange term is treated implicitly through the block matrix. Thus, the term proportional to $q_{ie,j}(T_{e,j} - T_{i,j})$ contributes to the electron and ion diagonal blocks and to the corresponding off-diagonal electron-ion coupling blocks.

The coefficients in Eqs. 9-11 contain the stabilized conductivity

$$\hat{\chi}_{e,j+1/2} = \chi_{e,j+1/2} + \chi_{e,j+1/2}^{\text{stab}}$$

where $\chi_{e,j+1/2}$ is the physical electron thermal diffusivity provided by the selected transport model, while $\chi_{e,j+1/2}^{\text{stab}}$ is a numerical stabilization parameter. In the present implementation,

$$\chi_{e,j+1/2}^{\text{stab}} = \max\left(f_{\chi,e} \chi_{e,j+1/2}^{\text{ref}}, \chi_e^{\text{min}}\right),$$

where $f_{\chi,e}$ and χ_e^{min} are user-controlled numerical parameters, and $\chi_{e,j+1/2}^{\text{ref}}$ is the local reference diffusivity used to scale the stabilization. The quantity χ_e^{stab} is not an additional physical transport coefficient. Rather, it enters the finite-difference operator to regularize the nonlinear solve in regions where the transport coefficients or profile gradients vary rapidly. The maximum number of Newton iterations is specified by the user.

At the domain boundaries ($j = 1$ and $j = N$), the coefficients of the tridiagonal system are modified to impose boundary conditions on the electron temperature. At the inner boundary ($j = 1$), a zero-gradient (Neumann) condition is imposed:

$$T_{e,2} = T_{e,1},$$

which is implemented in the matrix system as:

$$A_1 = -1, \quad B_1 = 1, \quad C_1 = 0, \quad D_1 = 0,$$

enforcing $-T_{e,1} + T_{e,2} = 0$. At the outer boundary ($j = N$), a Dirichlet condition is applied:

$$A_N = 0, \quad B_N = 1, \quad C_N = 0, \quad D_N = T_{e,\text{bdr}},$$

where $T_{e,\text{bdr}}$ is a specified boundary temperature at the plasma edge.

The same stabilization parameter also enters the modified Péclet number used to control the upwind/central weighting of the face-centered transport operator:

$$\hat{P}_{e,j+1/2} = \frac{\left[V_{\text{conv},j+1/2} + \chi_{e,j+1/2}^{\text{stab}} (T'_e/T_e)_{j+1/2} \right] \Delta_{j+1/2}^r}{\chi_{e,j+1/2} + \chi_{e,j+1/2}^{\text{stab}}}.$$

This expression differs from the conventional Péclet number

$$P_{e,j+1/2} = \frac{V_{\text{conv},j+1/2} \Delta_{j+1/2}^r}{\chi_{e,j+1/2}},$$

because it includes the additional numerical scale χ_e^{stab} . This form makes the stabilization sensitive to the normalized profile gradient when the transport coefficients are small, rapidly varying, or strongly gradient-dependent. The modified Péclet number is then passed to the nonlinear stabilization function $F(\hat{P}_e)$, which appears directly in the discrete coefficients of the implicit solve:

$$F(x) = \begin{cases} -x, & x < -10, \\ (1 + 0.1x)^5 - x, & -10 \leq x < 0, \\ (1 - 0.1x)^5, & 0 \leq x < 10, \\ 0, & x \geq 10, \end{cases} \quad (13)$$

with $x = \hat{P}_e$. Figure 1 shows the plot of $F(x)$ versus $x = \hat{P}_e$.

The stabilization function varies nonlinearly with the modified Péclet number. In the limiting case of negligible physical convection and a stabilization scale that dominates the physical diffusivity, the modified Péclet number approaches a local normalized-gradient measure,

$$\hat{P}_{e,j+1/2} \simeq \left(\frac{T'_e}{T_e} \right)_{j+1/2} \Delta r_{j+1/2}.$$

Thus, the stabilization acts most strongly in zones with large normalized gradients or rapidly varying transport coefficients. The numerical scale entering this expression is controlled by `PT_SOLVER` input parameters and should be interpreted as a nonlinear stabilization device, not as an additional physical transport coefficient.

The residual at each grid point is defined as

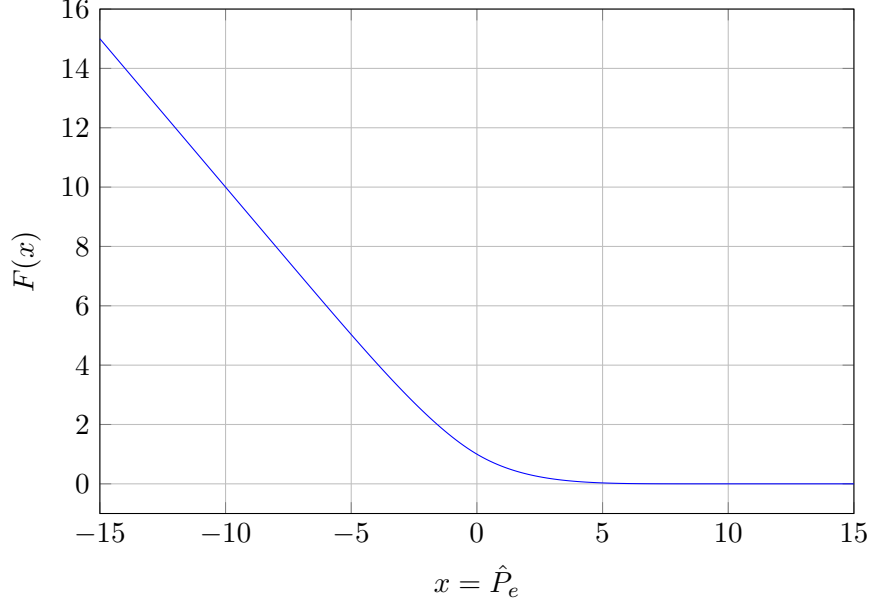


Figure 1: Plot of the stabilization function $F(x)$ versus $x = \hat{P}_e$. For $x \geq 10$, $F(x) = 0$; for x near 0, $F(x) \approx 1$; and for $x < -10$, $F(x) = -x$.

$$\mathfrak{R}_j = \frac{U_j^{n+1} - U_j^n}{\Delta t} + \frac{1}{V_j'} \left(\tilde{A}_j U_{j-1}^{n+1} + B_j U_j^{n+1} + \tilde{C}_j U_{j+1}^{n+1} \right) - S_j. \quad (14)$$

The L2 norm of the residual is then

$$\|\mathbf{R}\|_2 = \left(\sum_{j=1}^N \mathfrak{R}_j^2 \Delta \xi \right)^{1/2}. \quad (15)$$

To monitor convergence in the electron energy solver, PT_SOLVER evaluates the signed discrete energy-balance defect in each radial zone. We first define

$$Q_{1,j} = P_{e,j} - \frac{\partial(n_e T_e)_j}{\partial t} - Q_{ei,j} - Q_{\text{cmp},j} - Q_{\text{cmp,eldot},j} - Q_{\text{eldot},j}, \quad (16)$$

$$Q_{2,j} = Q_{e,j}^{\text{ext}} - Q_{e,j}^{\text{in}}, \quad (17)$$

where $P_{e,j}$ is the zone-integrated external power input to electrons, including contributions from neutral beam injection, recycling, and alpha-particle heating; $\partial(n_e T_e)_j / \partial t$ is the time derivative of the electron energy density in zone j with $n_e T_e$ representing the electron energy density; $Q_{ei,j}$ is the collisional energy exchange between electrons and ions; $Q_{\text{cmp},j}$ represents the plasma compression due to plasma volume change:

$$Q_{\text{cmp},j} = \frac{k_B n_{e,j} T_{e,j}}{\Delta t} \left(V_j - V_j^{(n)} \right) \quad (18)$$

$Q_{\text{cmp,eldot},j}$ is the grid-motion correction to the compression term due to grid motion-induced volume change:

$$Q_{\text{cmp,eldot},j} = k_B \dot{\xi} \left(\xi_{j+1} V_{j+1}' - \xi_j V_j' \right) n_{e,j} T_{e,j} \quad (19)$$

$Q_{\text{eldot},j}$ is the energy contribution from the net pressure work due to mesh velocity:

$$Q_{\text{eldot},j} = -\frac{3}{2}k_B\dot{\xi} \left(\xi_{j+1}V'_{j+1} \frac{n_{e,j}T_{e,j} + n_{e,j+1}T_{e,j+1}}{2} - \xi_jV'_j \frac{n_{e,j-1}T_{e,j-1} + n_{e,j}T_{e,j}}{2} \right) \quad (20)$$

$Q_{e,j}^{\text{ext}}$ and $Q_{e,j}^{\text{in}}$ are the transport fluxes evaluated at the exterior and interior boundaries of zone j , respectively. Their difference $Q_{2,j}$ provides the net transport contribution across the zone.

The local electron energy-balance defect is then

$$\epsilon_{e,j} = Q_{2,j} - Q_{1,j}, \quad (21)$$

and the corresponding unsigned local power budget used for normalization is

$$B_{e,j} = |Q_{e,j}^{\text{ext}}| + |Q_{e,j}^{\text{in}}| + |P_{e,j}| + \left| \frac{\partial(n_e T_e)_j}{\partial t} \right| + |Q_{ei,j}| \quad (22)$$

$$+ |Q_{\text{cmp},j}| + |Q_{\text{cmp,eldot},j}| + |Q_{\text{eldot},j}|. \quad (23)$$

The normalized electron-temperature residual is defined as

$$\mathbb{R}_{T_e} = \frac{\left(\sum_{j=1}^N \epsilon_{e,j}^2 \right)^{1/2}}{\max \left[\left(\sum_{j=1}^N B_{e,j}^2 \right)^{1/2}, B_{\text{floor}} \right]}. \quad (24)$$

A pointwise residual may also be monitored as

$$r_{T_e,j} = \frac{|\epsilon_{e,j}|}{\max(B_{e,j}, B_{\text{floor}})}. \quad (25)$$

Here B_{floor} is a small positive floor that prevents division by zero in zones where all terms in the local balance are negligible. This formulation measures the normalized defect of the signed discrete conservation law. The normalization is based on the unsigned local power budget rather than on the sum of two signed net quantities, avoiding artificial saturation when the source/time-derivative side and the transport-flux side have opposite signs.

The fluxes $Q_{e,j}^{\text{ext}}$ and $Q_{e,j}^{\text{in}}$ entering Eqs. (21)–(25) are evaluated from the same face-centered discrete operator that is used to construct the implicit tridiagonal system. Thus, when modified-Péclet stabilization is enabled, the residual is formed using the stabilized numerical flux, not by recomputing the flux from only the unstabilized physical conductivity. Schematically, the numerical flux used in the nonlinear solve may be written as

$$Q_{e,j+1/2}^{\text{num}} = Q_{e,j+1/2}^{\text{phys}} + Q_{e,j+1/2}^{\text{stab}}$$

where $Q_{e,j+1/2}^{\text{phys}}$ contains the physical conductive and convective terms, while $Q_{e,j+1/2}^{\text{stab}}$ denotes the contribution introduced by the modified-Péclet discretization through χ_e^{stab} and $F(\hat{P}_e)$. The residual used for nonlinear convergence is therefore the defect of the stabilized discrete conservation law,

$$\epsilon_{e,j} = \left(Q_{e,j}^{\text{num,ext}} - Q_{e,j}^{\text{num,in}} \right) - Q_{1,j}.$$

This choice ensures that convergence is tested against the same algebraic system that is being solved. A residual reconstructed from Q_e^{phys} alone is still useful as a diagnostic of the size of the

stabilization correction and of the physical power-balance closure, but it is not the residual of the nonlinear discrete problem when stabilization is active.

The same consistency requirement applies to the moving-grid and compression terms: the face interpolation used in the residual reconstruction is kept identical to that used in the implicit coefficient assembly, so that the residual vanishes for a converged solution of the discretized equations up to solver tolerance.

Residuals are determined separately for each transport channel. Similarly, the profile change ratio \mathfrak{C}_i is calculated for each channel that is predicted, with \mathfrak{C}_{\max} being equal to $\max_i(\mathfrak{C}_i)$. Convergence of the nonlinear iteration is established if $\mathfrak{C}_{\max} < \mathfrak{C}_s$ and $\mathbb{R}_i < \mathfrak{r}_i$ for each transport channel i , where \mathfrak{r}_i is the user-defined threshold value for residual for channel i , and \mathfrak{C}_s is the threshold value for the maximum allowable profile change ratio.

For production runs, convergence depends on the simultaneous satisfaction of channel-specific residual tolerance criteria as well as the maximum profile change criteria. In order to increase robustness in the context of long-term simulation prediction runs, PT_SOLVER contains fail-safe procedures for those cases in which the adaptive time stepping procedure approaches the minimum time step specified by the user. In such situations, the solver can take a time step that meets an explicitly stated emergency criterion, on condition that profile changes are bounded and residuals do not exceed channel-specific multiples of the standard tolerances. Such time steps are tagged in the output and should be distinguished from steps satisfying the standard nonlinear convergence criterion. They are not used to define the strict convergence behavior reported in the verification tests.

4.2 Testing the Convergence of the Numerical Algorithm

In order to test the numerical convergence of the PT_SOLVER numerical scheme, we have developed a Python script that solves a simplified family of coupled one-dimensional nonlinear transport equations designed to reproduce the main numerical features of PT_SOLVER, including multi-channel coupling, implicit time advancement, Newton iterations, and modified-Péclet stabilization. It is not intended to reproduce the full physical TRANSP formulation in flux-surface geometry, but rather to provide a flexible numerical testbed for studying stability, convergence, and coupling behavior. For reproducibility of the results, the Python script, its inputs, and outputs are uploaded to Princeton Data Commons and available for download using the URL shared at the end of this article in the Data Availability section.

The model equations can be written as

$$\frac{\partial U_m}{\partial t} + \frac{\partial}{\partial x} \left[-D_m(U, \partial_x U) \frac{\partial U_m}{\partial x} + v_m(U, \partial_x U) U_m - \dot{x} U_m \right] = S_m^{(\text{par})}(x, t) + \sum_{j \neq m} c_{mj} (U_j - U_m), \quad (26)$$

where $m = 1, \dots, M$.

Here, $U_m(x, t)$ is the m -th transport channel, D_m is the channel diffusivity, v_m is the convective velocity, \dot{x} is an optional mesh velocity term, $S_m^{(\text{par})}$ is the prescribed parametrized source, and c_{mj} are optional linear coupling coefficients between channels.

The two diffusivity models in the script are

$$D_m^{\text{linear}} = D_{0,m} + a_m \left| \frac{\partial U_m}{\partial x} \right|, \quad (27)$$

and

$$D_m^{\text{stiff}} = D_{0,m} + a_m \max\left(\left|\frac{\partial U_m}{\partial x}\right| - g_{\text{crit},m}, 0\right). \quad (28)$$

With stabilization enabled, the script actually uses an effective diffusivity

$$D_{m,\text{eff}} = D_m + \chi_m^{\text{stab}} F(\hat{P}_m), \quad (29)$$

with

$$\hat{P}_m = \frac{(v_m + \chi_m^{\text{stab}} \partial_x U_m / U_m) \Delta x}{D_m + \chi_m^{\text{stab}}}, \quad (30)$$

and the same piecewise stabilization function F defined in Sec. 4.1. The script is therefore aligned with the numerical idea of modified-Péclet stabilization, but in a simplified setting.

4.2.1 Analytical benchmark: coupled diffusion with constant exchange

To verify the numerical implementation, we consider a two-channel linear transport problem for electron and ion temperatures, $T_e(x, t)$ and $T_i(x, t)$, on the interval $0 \leq x \leq L$, with constant diffusivities and symmetric inter-channel relaxation:

$$\frac{\partial T_e}{\partial t} = D \frac{\partial^2 T_e}{\partial x^2} + \alpha (T_i - T_e), \quad (31)$$

$$\frac{\partial T_i}{\partial t} = D \frac{\partial^2 T_i}{\partial x^2} + \alpha (T_e - T_i), \quad (32)$$

where D is the constant diffusivity and α is the coupling coefficient.

Homogeneous Dirichlet boundary conditions are imposed at both ends of the domain,

$$T_e(0, t) = T_e(L, t) = 0, \quad T_i(0, t) = T_i(L, t) = 0,$$

and the initial conditions are chosen as a single sinusoidal mode,

$$T_e(x, 0) = A_e \sin(kx), \quad T_i(x, 0) = A_i \sin(kx), \quad k = \frac{n\pi}{L}.$$

It is convenient to introduce the sum and difference variables

$$S = T_e + T_i, \quad \Delta = T_e - T_i.$$

Substituting Eqs. (31)–(32) gives two decoupled equations,

$$\frac{\partial S}{\partial t} = D \frac{\partial^2 S}{\partial x^2}, \quad \frac{\partial \Delta}{\partial t} = D \frac{\partial^2 \Delta}{\partial x^2} - 2\alpha \Delta.$$

Since the initial condition contains only a single eigenmode, the exact solution remains proportional to $\sin(kx)$ for all time:

$$S(x, t) = (A_e + A_i) e^{-Dk^2 t} \sin(kx), \quad \Delta(x, t) = (A_e - A_i) e^{-(Dk^2 + 2\alpha)t} \sin(kx).$$

The exact solutions for the two channels then follow from $T_e = (S + \Delta)/2$ and $T_i = (S - \Delta)/2$:

$$T_{e,i}(x, t) = \frac{1}{2} \left[(A_{e,i} + A_{i,e}) e^{-Dk^2 t} \pm (A_{e,i} - A_{i,e}) e^{-(Dk^2 + 2\alpha)t} \right] \sin(kx),$$

For the specific parameters given in the caption to Fig. 2, the solution becomes

$$T_{e,i}(x, t) = \left[0.6 e^{-0.9\pi^2 t} \pm 0.4 e^{-(0.9\pi^2 + 10)t} \right] \sin(3\pi x),$$

The results of numerical and analytical solution comparison are shown in Fig. 2. This benchmark is useful because it tests both diffusion and coupled relaxation in a setting with a closed-form analytical solution. The common mode, $S = T_e + T_i$, decays purely by diffusion, while the difference mode, $\Delta = T_e - T_i$, decays faster due to both diffusion and inter-channel exchange.

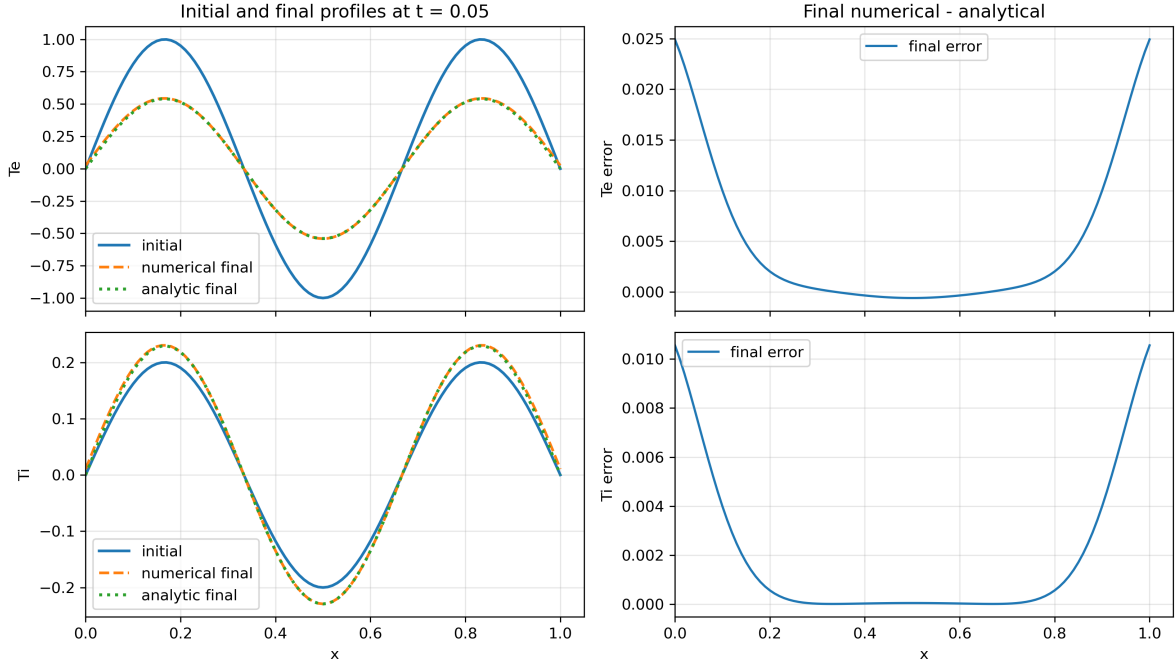


Figure 2: Initial and final profiles for the constant-diffusivity coupled benchmark with the following parameters: $L = 1$, $n = 3$, $D = 0.10$, $\alpha = 5.0$, $A_e = 1.0$, $A_i = 0.2$, and $k = 3\pi$. Shown are the initial electron and ion temperature profiles and the corresponding numerical solutions at the final time. The profile evolution is governed by constant diffusion together with symmetric electron–ion relaxation, so that both overall decay and equilibration between channels are visible. The left panels show the initial, final, and analytical solutions for electron and ion temperature profiles, and the right panels show the absolute errors between the numerical and analytical solutions.

4.2.2 Manufactured-solution test with evolving H-mode pedestal

The previous test demonstrates that the coupled diffusion equations evolved to the analytical solution. However, the problem was formulated using simple sinusoidal profiles with homogeneous boundary conditions, which are far from any experiment-relevant observations.

To verify the coupled transport solver for profile shapes more representative of tokamak applications, we consider a method-of-manufactured-solutions (MMS) test for electron and ion temper-

atures, $T_e(x, t)$ and $T_i(x, t)$, on the interval $0 \leq x \leq L$. The governing equations are

$$\frac{\partial T_e}{\partial t} = D_e \frac{\partial^2 T_e}{\partial x^2} + \alpha (T_i - T_e) + S_e(x, t), \quad (33)$$

$$\frac{\partial T_i}{\partial t} = D_i \frac{\partial^2 T_i}{\partial x^2} + \alpha (T_e - T_i) + S_i(x, t), \quad (34)$$

where D_e and D_i are constant diffusivities and α is the inter-channel relaxation coefficient.

The exact manufactured solutions are chosen as H-mode-like profiles with a time-dependent pedestal amplitude and an additional decaying sinusoidal perturbation,

$$T_m^M(x, t) = T_{m,\text{ped}} + \Delta_m(t) H(x) + a_m e^{-\lambda_m t} \sin(k_m x), \quad m \in \{e, i\}, \quad (35)$$

with

$$H(x) = \frac{1}{2} \left[1 - \tanh\left(\frac{x - x_{\text{ped}}}{w}\right) \right], \quad (36)$$

$$\Delta_m(t) = \Delta_{m,0} + \Delta_{m,1} \left(1 - e^{-\beta_m t} \right),$$

and $k_m = n_m \pi / L$.

The pedestal shape is controlled by the fixed function $H(x)$, while its amplitude evolves in time through $\Delta_m(t)$. The sine term provides an additional smooth perturbation that decays exponentially in time.

The source terms are constructed analytically by substituting the manufactured solutions into Eqs. (33)–(34),

$$S_e(x, t) = \frac{\partial T_e^M}{\partial t} - D_e \frac{\partial^2 T_e^M}{\partial x^2} - \alpha (T_i^M - T_e^M), \quad (37)$$

$$S_i(x, t) = \frac{\partial T_i^M}{\partial t} - D_i \frac{\partial^2 T_i^M}{\partial x^2} - \alpha (T_e^M - T_i^M). \quad (38)$$

To evaluate these expressions, note that $\dot{\Delta}_m(t) = \Delta_{m,1} \beta_m e^{-\beta_m t}$, and, with $\eta = (x - x_{\text{ped}})/w$, the second derivative of the pedestal shape is

$$H''(x) = \frac{1}{w^2} \text{sech}^2(\eta) \tanh(\eta).$$

Therefore,

$$\frac{\partial T_m^M}{\partial t} = \dot{\Delta}_m(t) H(x) - \lambda_m a_m e^{-\lambda_m t} \sin(k_m x), \quad (39)$$

$$\frac{\partial^2 T_m^M}{\partial x^2} = \Delta_m(t) H''(x) - a_m k_m^2 e^{-\lambda_m t} \sin(k_m x). \quad (40)$$

The benchmark is solved with exact Dirichlet boundary conditions,

$$T_e(0, t) = T_e^M(0, t), \quad T_e(L, t) = T_e^M(L, t), \quad T_i(0, t) = T_i^M(0, t), \quad T_i(L, t) = T_i^M(L, t),$$

and with initial conditions taken directly from the manufactured solution at $t = 0$,

$$T_e(x, 0) = T_e^M(x, 0), \quad T_i(x, 0) = T_i^M(x, 0).$$

In the present test, the numerical values are

$$L = 1, \quad x_{\text{ped}} = 0.82, \quad w = 0.04,$$

$$D_e = 0.05, \quad D_i = 0.03, \quad \alpha = 3.0,$$

and

$$\begin{aligned} T_{e,\text{ped}} &= 0.30, & \Delta_{e,0} &= 0.55, & \Delta_{e,1} &= 0.40, & \beta_e &= 20.0, & a_e &= 0.08, & \lambda_e &= 6.0, & n_e &= 2, \\ T_{i,\text{ped}} &= 0.18, & \Delta_{i,0} &= 0.35, & \Delta_{i,1} &= 0.28, & \beta_i &= 14.0, & a_i &= -0.06, & \lambda_i &= 5.0, & n_i &= 3. \end{aligned}$$

The simulation is performed on a uniform grid with

$$N_x = 201, \quad \Delta t = 10^{-4}, \quad t_{\text{final}} = 5 \times 10^{-2}.$$

The results of our test are summarized in Fig. 3. This MMS test is more demanding than a single-mode diffusion benchmark because it combines nontrivial H-mode-like spatial structure, time-dependent pedestal evolution, inter-channel coupling, and analytically known source terms. It therefore provides a stringent verification case for both the spatial discretization and the time advancement of the coupled solver.

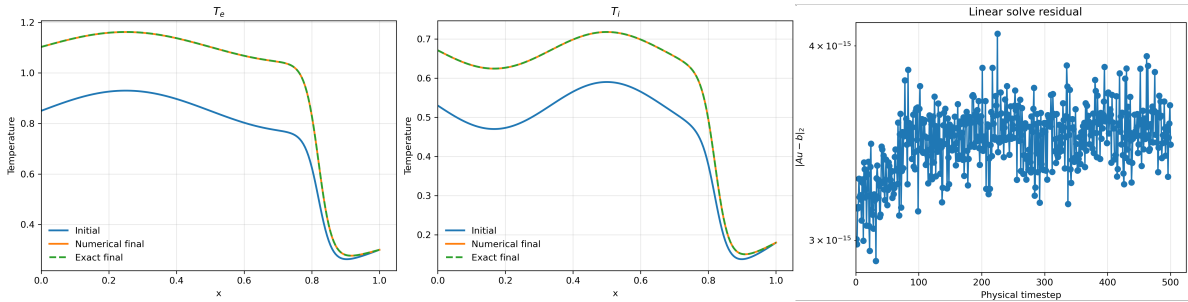


Figure 3: MMS benchmark with evolving H-mode-like pedestal profiles. Left and middle panels compare the initial profiles with the numerical and exact manufactured solutions at the final time for the electron and ion temperature channels, respectively. The benchmark combines constant diffusivities, inter-channel relaxation, exact source balancing, and time-dependent pedestal amplitudes, so that the full profile shape evolves while remaining analytically prescribed. The numerical and exact final profiles are nearly indistinguishable on the scale of the plot, indicating accurate reproduction of the manufactured solution. The right panel shows the residual of the linear solve at each physical time step, demonstrating stable and well-converged implicit advancement throughout the simulation.

4.2.3 Numerical test for the model with gradient-dependent diffusivities

Physics-based models for anomalous transport incorporate the dependence of effective diffusivities on plasma gradients. Typically, the dependence is nonlinear. A particular case of effective diffusivity that depends linearly on plasma gradients and has a stability threshold can be described with this expression:

$$D_m^{\text{stiff}} = D_{0,m} + a_m \max\left(\left|\frac{\partial U_m}{\partial x}\right| - g_{\text{crit},m}, 0\right). \quad (41)$$

In this expression, $D_{0,m}$ is the minimal diffusivity that is always present and independent of the plasma gradients $\partial U_m / \partial x$, $g_{\text{crit},m}$ is the critical gradient level that represents the threshold of instability that drives the anomalous transport, and a_m is the stiffness coefficient. This stiff transport model is representative of a wide class of drift-wave instabilities in tokamaks. There is no exact analytical solution for this case, and we present results of convergence studies for a particular selection of diffusivities in coupled plasma profile equations.

The results obtained in this test for coupled transport equations, as shown in Figs. 4 and 5, demonstrate stable nonlinear convergence and physically correct redistribution for all three transport channels in the simulation that combine sources, diffusion, and cross-channel coupling. In this test case, both the electron and ion temperature equations are coupled, while the plasma density channel evolves independently. The input file for this test case uses $N_x = 81$ radial points, $\Delta t = 5 \times 10^{-4}$, $t_{\text{final}} = 2 \times 10^{-2}$, and up to 100 Newton iterations per time step, where both residual and relative change tolerances are set to 10^{-8} and nonlinear stabilization is enabled. The electron and ion temperature channels are initialized using Gaussian profiles and use an off-axis Gaussian source term and stiff diffusion, while the plasma density channel is initialized using a Gaussian profile and uses a parabolic source term localized at the plasma edge and stiff diffusion. Zero gradient boundary conditions are used at the magnetic axis, while constant boundary conditions are set for the outer boundary with $T_e = 0.6$, $T_i = 0.5$, and $n = 0.9$. The temperature coupling matrix only includes off-diagonal elements $c_{ei} = c_{ie} = 8$. As a result, only electron-ion temperature relaxation is allowed without any coupling to plasma density. The profiles evolve smoothly into broader and less peaked shapes, and the strongest coupling effect is seen in the temperature channels. The convergence histories show monotonically decreasing maximum residual and relative change, as required for nonlinear convergence in PT_SOLVER, and demonstrate the expected behavior that decreasing physical time steps require fewer and less severe Newton iterations for convergence.

As a further illustration, the sensitivity of nonlinear convergence to the physical time step and the stiffness in the gradient-dependent transport model is demonstrated in Fig. 5. The residual is always reduced monotonically as the solver converges using the Newton iterations, and this is true in all cases considered here, at both the initial and final time steps. The effect of the stiffness is clearly demonstrated, as the reduced stiffness case shows faster convergence with a smaller number of iterations and a faster rate of residual reduction, whereas the higher stiffness case shows a slower rate of residual reduction and a greater number of iterations. The latter is consistent with the form of the model diffusivity in Eq. 41, as the sensitivity of the effective transport to local gradients is increased as the stiffness is increased, thus making the problem more nonlinear in the implicit solver. The results confirm the PT_SOLVER convergence in the full range of the parameter sweep, and they also confirm that higher stiffness has a significant impact on the nonlinear solver.

Although the theory-based model may be expected to be less prone to the effects of anomalous transport coefficients than the explicit stiffness model, the numerical problem related to the stiffness in the transport coupled equations still persists in the sense that the transport coefficients may be

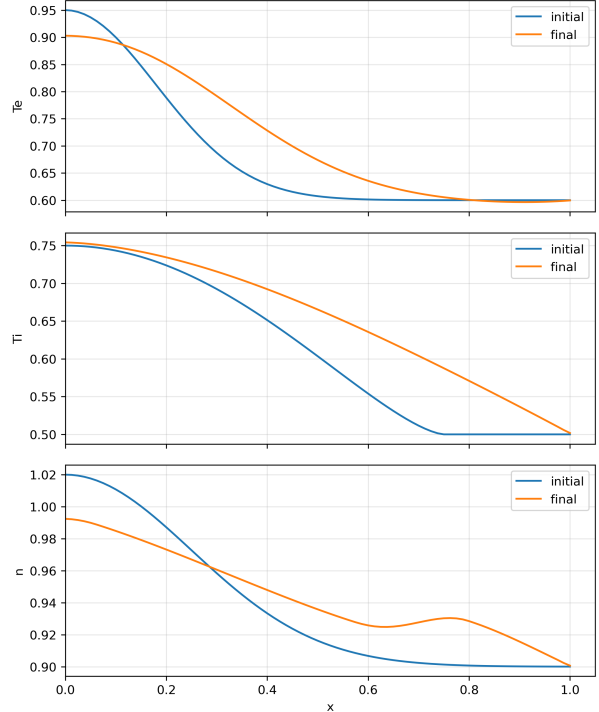


Figure 4: Profiles evolution for the coupled three-channel transport test at initial and final time steps. Results are shown for four physical time steps, $\Delta t = 5 \times 10^{-4}$, 10^{-3} , 2×10^{-3} , and 10^{-2} . The results converge to the same final states independent of the physical time steps. The residuals for different iterations are shown in the left panels of Fig. 5.

significantly influenced by the evolving profiles, and this is a problem that is common in a wide range of applications involving the simulation of the transport of reacting systems, as the transport coefficients may be significantly influenced by the evolving profiles in the reactions and the diffusion processes. The numerical problem is therefore not so much related to the explicitness of the stiffness, but rather whether the transport model itself is nonlinear in the solver.

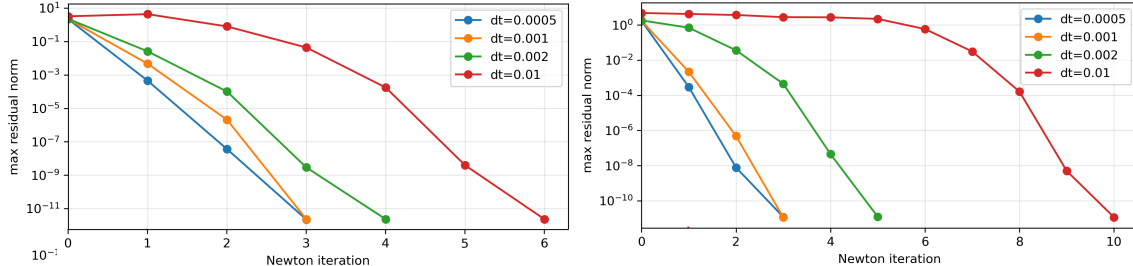


Figure 5: The maximum residual norms over all transport channels as a function of Newton iteration at the first and final time steps. Results are shown for two stiffness coefficients $a_{Te/Ti/ne} = (0.2, 0.2, 0.4)$ (left) and $a_{Te/Ti/ne} = (2, 2, 4)$ (right) and four physical time steps, $\Delta t = 5 \times 10^{-4}$, 10^{-3} , 2×10^{-3} , and 10^{-2} . In all cases, the nonlinear iterations converge rapidly, and the smaller time steps exhibit faster reduction of residuals. The comparison between the first and fortieth physical steps indicates that the coupled solve remains robust after the profiles have evolved away from their initial conditions. The large stiffness makes convergence more difficult.

For realistic predictive calculations, the nonlinear transport problem may be more complex than that treated in this idealized stiffness scan. As mentioned in this paper, theory-based transport models are generally functions of multiple and competing gradients rather than a single control parameter. For example, in the thermal transport driven by the ion temperature gradient modes, the destabilizing effect of the ion temperature gradient and the stabilizing effect of the density gradient are coupled in such a way that the rate of evolution to marginal stability is determined by a complex interplay between these two gradients rather than by the monotonically changing value of a single gradient. As a result, the stiffness of the transport response can vary significantly in both space and time and may change rapidly in response to changing profiles. Another complication in realistic TRANSP calculations is that not all profiles are self-consistently evolved in response to plasma evolution. Some profiles may be provided as inputs based on experimentally determined fits to analogous plasmas or external models. In stiff transport calculations, this noise is undesirable because it directly affects local gradients used in determining transport coefficients and may lead to undesirable oscillations in local diffusivities, which would degrade nonlinear convergence.

Beyond the parallel scaling strategy described above, PT_SOLVER also addresses the practical cost of predictive simulations through the modular design of its transport-model interface. Because the solver advances the transport equations separately from the internal details of a particular transport model, the same framework can be coupled not only to standard reduced theory-based models but also to machine-learning surrogates of those models. This feature becomes especially crucial when the predictive simulations demand small physical time steps or extended pulse lengths, since repeated evaluations of the computationally costly transport models could become too expensive. In this sense, PT_SOLVER provides a pathway for incorporating transport physics of different fidelity into integrated modeling workflows without sacrificing numerical robustness or practical turnaround time.

4.3 Verification with the TGYRO code

The use of stiff turbulence models for cross-verification of transport solvers presents a challenge because the transport fluxes are determined based on local profile gradients as well as the specific details of the magnetic equilibrium, which include both the q -profile and magnetic shear. In addition to the gradients, these quantities can play a critical role in the transport level predicted with the models. Small differences in the numerical representation of equilibrium or from the interpolation of input data and sources can lead to significant differences in profile predictions and, in some cases, result in a different branch of instability driving the anomalous transport. Therefore, for the cross-verification of two predictive solvers, both solvers must be aligned as much as possible and use the same equilibrium, boundary conditions, and sources so that the two transport model inputs are consistent. Therefore, in order to limit any differences unrelated to the transport solver being verified (e.g., to limit differences between the two transport solvers being compared), both PT_SOLVER and TGYRO use the equilibria reconstructed from experiment rather than evolving them in a self-consistent manner.

In DIII-D H-Mode discharge 125236, PT_SOLVER and TGYRO predict similar transport behavior for the majority of their predictive region from $\rho = 0$ to $\rho = 0.8$ where the boundary conditions were set. Both codes use the TGLF model [35, 51, 52] for the anomalous transport and the NEO model [53] for the neoclassical transport. Experimental profiles are included for reference. The vertical dotted line at $\rho = 0.8$ represents the edge of the predictive region.

The largest differences between solvers are observed for the electron temperature in the core, while the ion temperature and the electron density are more consistent. It appears that both solvers predict the electron temperatures above the experimental values. Since this benchmark uses a common transport-model setup but is not fully self-consistent, the over-prediction of T_e relative to experiment should be attributed to the shared model configuration rather than to differences between the two solvers. The remaining difference between PT_SOLVER and TGYRO is plausibly related to differences in solver formulation, including the time-dependent evolution in PT_SOLVER versus the steady-state flux-matching approach in TGYRO, together with differences in source interpolation and other workflow details. However, despite the differences in the electron

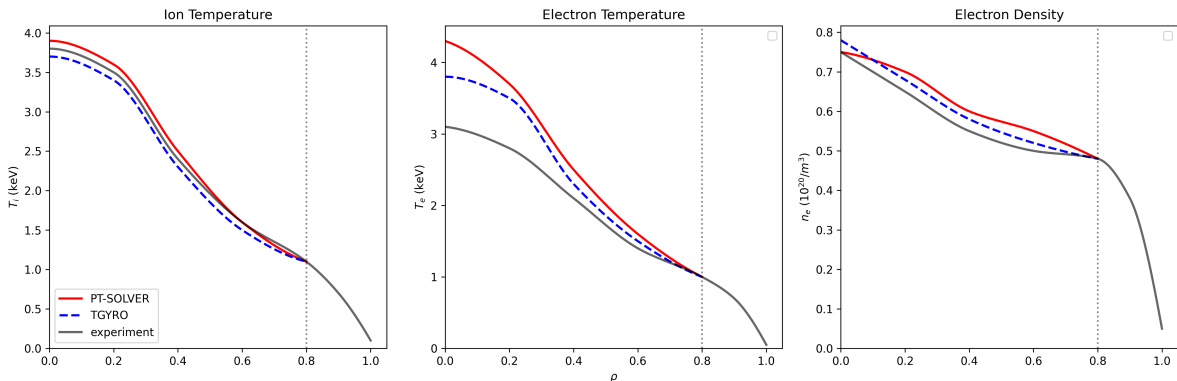


Figure 6: Comparison of standalone PT_SOLVER and TGYRO results for the DIII-D H-mode discharge 125236 using TGLF for anomalous transport and NEO for neoclassical transport in both workflows. Red solid curves denote PT_SOLVER, blue dashed curves denote TGYRO, and gray curves denote the experimental profiles. The dotted vertical line at $\rho = 0.8$ marks the outer boundary of the predictive region. The agreement is generally good for T_i and n_e , while the largest difference is observed for T_e in the inner core.

temperature predictions from PT_SOLVER and TGYRO, they are still in agreement with each other for the most part of the profile.

For the purposes of the present paper, these results should be regarded as solver and workflow verification rather than comprehensive model validation. Specifically, this research does not have an objective to establish predictive accuracy or fidelity using experimental data, so there is no way to evaluate whether the TGLF and NEO predictions are accurate based on such tests. At the same time, recent database-oriented studies, including DIII-D, MAST-U, and NSTX comparisons [8, 10, 11, 54], have addressed validation of related reduced-model and predictive workflows and provide important complementary context, but those studies are outside the scope of the present paper. The analysis in this paper shows that the profile predictions produced by PT_SOLVER are consistent with the TGYRO results, provided that the equilibrium, source terms, and boundary conditions are controlled as closely as possible. This verification test supports the conclusion that PT_SOLVER is numerically consistent with the reference workflow for the matched TGLF/NEO benchmark configuration.

4.4 Multilevel parallelization strategy and scaling

PT_SOLVER is designed as a parallel modular solver with multiple levels of parallelization. The nonlinear profile advance and the expensive transport-model evaluations can be decomposed across multiple levels of parallel communication. The MPI_COMM_WORLD communication pattern shown in the diagram in Fig. 7 has been divided into multiple sub-communicators, one per flux surface. The implementation is shown on an example of the TGLF model that maintains its own parallelization across different wavenumbers. The global communicator, MPI_COMM_WORLD, is partitioned into sub-communicators, MPI_GRP_ i , associated with individual radial flux surfaces. Within each sub-communicator, processors are assigned to the parallel evaluation of TGLF over wavenumber space, denoted here by k_0, \dots, k_n . These calculations are associated to individual PEn, or n -th MPI process ranks. This two-level decomposition enables simultaneous parallelization over flux surfaces and over the internal TGLF calculation at each surface. The transport coefficients computed using these transport model calculations are collected and passed back to the Newton iteration for the transport equation advancement. The resulting architecture enables scalable processor use beyond just being limited to the number of radial zones, thereby increasing the effective use of both radial and k_y spatial concurrency.

The scaling results that correspond to this implementation are shown in Fig. 8. The first scaling data set indicates that TGLF has a reasonable scaling up to the limits of n_{ky} decomposition. The second plot in Fig. 8 corresponds to the conditions where the number of zones is greater than the number of CPUs so that PT_SOLVER and TGLF operate in parallel; however, PT_SOLVER creates only one sub-communication group, and internal parallelization over wavenumbers inside TGLF is used. The third scaling plot in Fig. 8 indicates a condition where the number of zones is less than the number of CPUs, so that both PT_SOLVER and TGLF are performing in parallel mode. The three scaling examples demonstrate the automatic transition of the two workflow modes of operation for PT_SOLVER and TGLF: PT_SOLVER op-

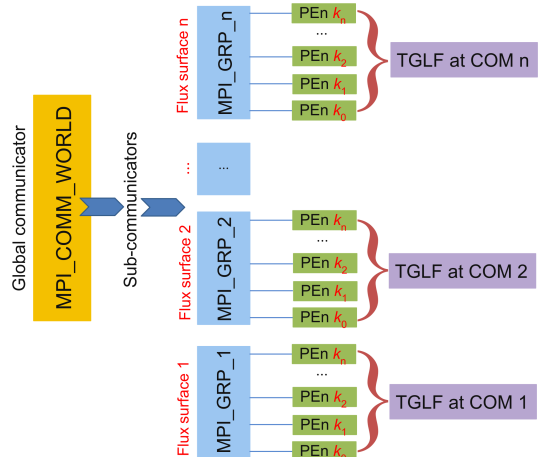


Figure 7: Schematic illustration of the multilevel parallelization strategy used in PT_SOLVER for coupled transport calculations with TGLF.

erating in parallel mode and TGLF operating in serial mode, when the radial workload is primarily located within one or more transport zones, and both PT_SOLVER and TGLF operating in parallel mode, when additional CPUs are available beyond the total number of zones in the transport; thus allowing for efficient use of available CPU resources.

The scope of this PT_SOLVER verification should be limited to the presented benchmark hierarchy. The objective of this verification is to confirm the numerical convergence of the predictive solver, and the correctness of the interface implementation and the associated workflow, not to provide a comprehensive validation of all transport models available in TRANSP. In particular, the simplified gradient-dependent diffusivity tests are used solely to isolate the stiffness and convergence characteristics of the nonlinear solver, while the TGYRO comparisons are meant to confirm that both the solver and the workflow are consistent with TGLF and NEO inputs. However, we are not evaluating the predictive accuracy compared to experimental data. The multilevel scaling findings are an indication of the PT_SOLVER/TGLF interface and must not be used as a general performance metric for all model combinations. The verification here focuses specifically on the channels and workflow that are exercised in the benchmark set to show how robust the current numerical schema is under these conditions. Overall validation, along with additional evaluations of frameworks, will be conducted in the future.

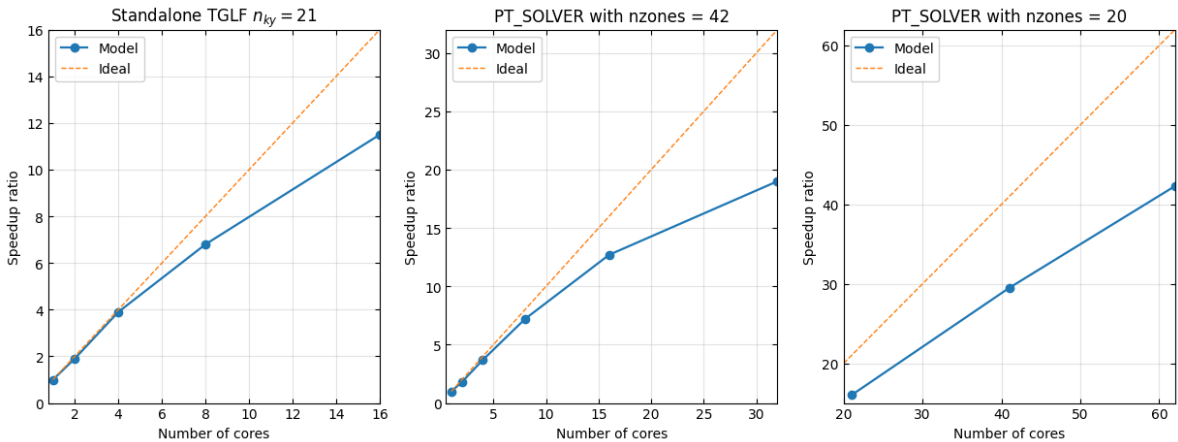


Figure 8: Parallel scaling of the PT_SOLVER with the TGLF model for three representative configurations. Left: scaling of standalone TGLF with $n_{ky} = 21$. Middle: scaling of PT_SOLVER TGLF for $n_{zones} = 42 > N_{cores}$. Right: scaling of PT_SOLVER with parallel TGLF for $n_{zones} = 20 < N_{cores}$. In each panel, the solid curve shows the measured model speedup, and the dashed line indicates ideal linear scaling. Standalone TGLF exhibits good scaling up to the number of processors comparable to the number of k_y modes, while PT_SOLVER benefits from an additional level of parallelism over transport zones. When both levels of parallelism are used simultaneously, the combined workflow maintains substantial speedup, although with the expected departure from ideal scaling due to communication and load-balance overheads.

5 Implementation of T3D/GX in TRANSP for Gyrokinetic Turbulence Simulations

T3D is a transport solver developed in Python and designed to perform self-consistent macro-scale plasma profile evolution in a modular fashion, while the GX code represents a nonlinear gyrokinetic turbulence code designed to provide high-fidelity turbulent flux calculations on GPU architectures. The goal of this section is not to assert the physics validity of the coupled TRANSP/T3D/GX process. Instead, it is to describe the coupling process and to highlight the state information exchanged between the two codes and the verification process to ensure the correctness of the interface implementation. This is consistent with the verification of solvers presented in this work, where the focus is on the numerical correctness and integrity of the coupled process rather than the transport process itself, and comparison to experiment.

The justification behind connecting TRANSP to T3D/GX is not to replace the reduced theory-based models available through PT_SOLVER. Rather, it is a step toward developing a flexible approach where selected cases using reduced and high-fidelity models can be compared within the same modeling environment, using a common framework with the same interfaces and data structures. This capability is valuable for interface verification, assessment of reduced-model assumptions, and future hybrid workflows in which expensive turbulence calculations may be combined with surrogate or reduced descriptions for practical predictive applications.

The background and implementation of the GX code follow the Laguerre–Hermite representation developed by Mandell *et al.*, who showed that this representation provides a smooth interpolation between low-resolution gyrofluid-like and high-resolution gyrokinetic limits [23]. The recent publication of the current version of the GX code describes it as a gyrokinetic turbulence code designed to run on GPU architectures and describes the numerical design choices that provide rapid nonlinear flux calculations on a single or few GPUs [24]. The T3D code follows the multiscale paradigm of direct multiscale coupling between transport evolution and local turbulence calculations established in the TRINITY framework [32]. The recent flux-driven simulations using T3D in the context of recent predictive simulations, including STEP-oriented applications, also highlight the relevance of the T3D code in transport simulations rather than as a comparison code [55].

5.1 Integration in TRANSP

To minimize disruption to the existing predictive framework, the T3D/GX integration in TRANSP was organized around a narrow and explicit interface. TRANSP remains responsible for the integrated workflow: equilibrium handling, source calculation, boundary conditions, and top-level predictive control. The coupling layer exports geometry and state information, launches T3D with template-based inputs, and re-imports the evolved profiles. In practical terms, the operational interface follows the documented TRANSP coupled-run workflow in which `LPREDICTIVE_MODE=5` activates the T3D pathway and the run directory contains a TRANSP namelist together with inputs for the T3D (`T3D_template.in`) and GX (`GX_template.in`) codes [56]. The official guide also makes explicit that the T3D import mode for the coupled branch is `transp_realtime` [56].

A schematic representation of the TRANSP-T3D interface is shown in Fig. 9. The coupling uses exported geometry and state objects – specifically GEQDSK-like geometry, profile and source data, and template-driven run control – to keep the external solver pathway synchronized with the predictive TRANSP state. This choice is also consistent with the broader TRANSP philosophy of interfacing external components through explicit, traceable data objects rather than by duplicating physics logic in several locations [3].

In the coupled density-prediction branch, charge neutrality and effective charge are enforced

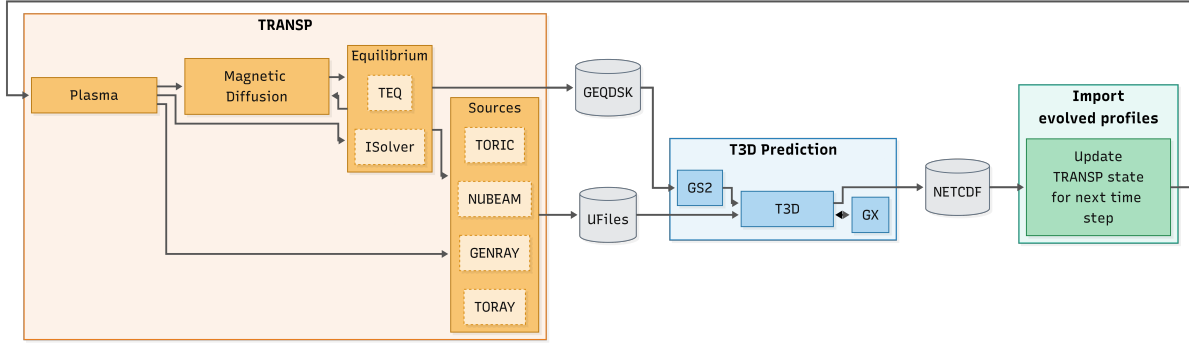


Figure 9: Interface-focused schematic of the TRANSP–T3D/GX coupling shows the modular organization and the direction of information exchange.

through

$$n_e = \sum_i n_i + \sum_{j,q} Z_q n_j^q, \quad (42)$$

$$n_e Z_{\text{eff}} = \sum_i n_i + \sum_{j,q} Z_q^2 n_j^q, \quad (43)$$

where the index i denotes singly charged main-ion species and n_j^q denotes the density of impurity species j in charge state q . These relations are applied during density prediction so that, for example, if electron density is evolved, the total thermal-ion density and impurity content can be reconstructed consistently from the known Z_{eff} while the fast-ion contribution is held fixed over the transport step. This makes explicit where consistency is enforced in the interface rather than leaving a reviewer to infer that the coupled branch might duplicate or silently modify these constraints. It also parallels the predictive-TRANSP statement that charge neutrality and Z_{eff} constrain density evolution in the native solver path [3].

A second point that deserves explicit clarification is the treatment of collisional electron–ion energy exchange. In predictive TRANSP/PT_SOLVER, collisional exchange appears as the term Q_{ei} in the electron and ion power-balance equations and enters the two channels with opposite signs, acting as a direct source for one species and an equal sink for the other [3]. In T3D, the same physical process is represented in the species pressure equations through a collisional relaxation operator of the form

$$\frac{\partial p_s}{\partial t} + \frac{1}{V'} \frac{\partial}{\partial \Psi} (V' Q_s) = \frac{3}{2} n_s \sum_u \nu_{su} (T_u - T_s) + S_{p,s}, \quad (44)$$

where the sum is over collisional partners u and the exchange coefficient is represented through ν_{su} [32, 55]. Thus, the coupled benchmarks do not compare two literally identical algebraic implementations. Instead, they verify that the interface maps the same underlying inter-species relaxation physics consistently between the native TRANSP formulation and the T3D formulation. This distinction is important because it explains why the $Q_{ei} = 0$ cases isolate pure interface bookkeeping, whereas the $Q_{ei} \neq 0$ cases additionally test consistency of the inter-channel coupling logic.

5.2 Verification of the TRANSP/T3D interface

The verification benchmark retained here is intended to answer a limited but important question: when T3D is connected through the TRANSP interface and supplied with matched inputs, does

the coupled interface reproduce the same profile evolution expected from the predictive TRANSP formulation for the benchmark considered? The answer from the present test set is yes, within the accuracy visible in the benchmark panels shown in Fig. 10. The benchmark results increase physics complexity in a controlled way. The first row removes auxiliary heating, diffusion, and collisional electron-ion exchange. The next rows introduce impurity content and Q_{ei} coupling, and the final row adds a source term while retaining the impurity and collisional structure. This progression is useful because it tests not only the transport advance itself but also the interface bookkeeping associated with source terms, impurity-aware density constraints, and collisional exchange.

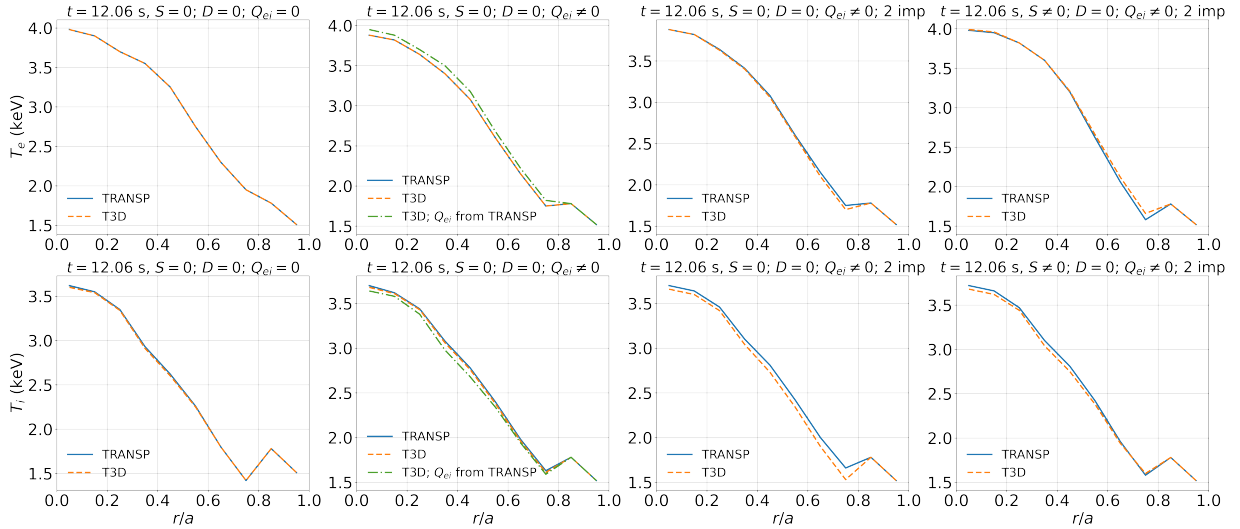


Figure 10: Comparison of predicted profiles using PT_SOLVER and T3D under different conditions. The benchmark is based on JET discharge 42982; because ion temperature measurements were unavailable, the electron temperature was used to set the ion-temperature boundary condition, producing an artificial initial discontinuity in T_i that serves here as a useful marker for electron-ion collisional coupling. The columns correspond to different test scenarios of increasing complexity, as indicated in the subplot titles (including variations in auxiliary heating S , number of impurities, and collisional energy exchange term Q_{ei}).

The first two columns show that the source-free cases preserve close agreement as impurity complexity and collisional exchange are introduced. The third column extends that check to the two-impurity case. The final column, which includes a nonzero source term, verifies that the coupled interface remains consistent once source handling is included.

The benchmark shown in Fig. 10 is based on the JET discharge 42982, which was used previously in TRINITY verification works. Ion-temperature edge data is not available for that discharge. Therefore, as is common practice in such situations, electron temperature is used as the basis for imposing the ion-temperature boundary condition. As a result, there appears an artificial discontinuity of the initial ion-temperature distribution at the predictive boundary. While this discontinuity is not physical, it is useful to verify our work as it provides us with an observable measure of the coupling between electron and ion channels through collisions. If $Q_{ei} = 0$, as seen in the first row of Fig. 10, the discontinuity appears only in the ion channel and no effect is visible in the electron channel. If the collisions are turned on, however, as seen in the other figures, the corresponding effect appears in both ion and electron channels.

Since the largest differences are likely associated with differences in the implementation of collisional energy exchange in PT_SOLVER and T3D, we briefly summarize those implementations

in PT_SOLVER and T3D here. In the T3D code, collisional energy exchange is treated using a fully multi-species formulation based on the fundamental expression

$$\frac{3}{2}n_s \sum_u \nu_{su} (T_u - T_s) \quad (45)$$

In this approach, the energy transfer for each species s is computed by explicitly summing over interactions with all other species u , with the coupling strength determined by the interspecies collision frequencies ν_{su} . This formulation naturally captures electron–ion, ion–ion, and impurity interactions within a unified framework and retains the detailed pairwise collisional physics. As such, it represents a more fundamental, kinetic-based description of energy exchange processes in a multi-component plasma.

In contrast, the TRANSP code employs a reduced model for electron–ion heat exchange, in which the detailed multi-species interactions are approximated through a lumped parameter. Specifically, the ion contribution is represented by a charge–mass weighted ion density of the form

$$\sum_s n_s \frac{Z_s^2}{A_s},$$

which enters the electron–ion coupling coefficient. This formulation is restricted to electron–ion interactions and avoids explicit summation over individual ion species by combining their effects into a single effective quantity. The weighting reflects the underlying collisional physics, with the Z_s^2 dependence enhancing the contribution of higher-charge ions and the $1/A_s$ factor accounting for the more efficient energy exchange associated with lighter ions. Consequently, TRANSP replaces the detailed, species-resolved collisional structure with an effective ion density that characterizes the aggregate coupling between electrons and the ion population.

Taken together, the benchmark Fig. 10 supports three specific claims. First, the interface preserves the expected mapping of predicted channels and imported channels across the coupled pathway. Second, the constraint logic required for density prediction is being applied consistently when impurities are present. Third, the treatment of collisional exchange and source bookkeeping does not introduce spurious differences between the two solver paths over the cases considered. What these panels do not demonstrate is broad transport-model validation; that would require a separate study against experimental observables or against underlying turbulence calculations over a broader database. However, PT_SOLVER in TRANSP and GX code in T3D, as well as GS2 code in TRINITY, have been verified before, and in this work, we verify only the numerical implementation of the interfaces. In other words, the present evidence should be read as interface verification and workflow verification, not as a general validation of T3D or GX physics performance.

The distinction matters for the scope of this paper. The present work is centered on predictive infrastructure in TRANSP and on the robustness of modular transport workflows. In that context, the TRANSP/T3D benchmark is valuable because it shows that the predictive framework can be extended in a controlled and traceable way to an external transport solver and, through it, to a high-fidelity turbulence model. This creates a practical path for future coupled studies with GX while keeping the present claims aligned with the evidence available.

5.3 Performance Considerations

One of the primary bottlenecks in these simulations arises from the computational intensity of resolving nonlinear gyrokinetic turbulence. These calculations necessitate high-resolution spatial and velocity grids, significantly increasing the numerical workload. Additionally, achieving accurate

turbulence evolution requires fine temporal resolution, which further increases the computational burden. As a result, even short-duration simulations demand substantial computational resources, making predictive studies difficult to execute within practical time constraints.

Another limiting factor is the available GPU memory, which imposes constraints on the scale of turbulence calculations. Large-scale turbulence simulations require substantial memory allocations, and the need to store multiple field quantities, distribution functions, and intermediate results can lead to bottlenecks when working within the limitations of current GPU architectures. These memory constraints can restrict the spatial resolution and physics fidelity of the simulations, potentially limiting the accuracy of long-duration transport predictions.

Although linear simulations for stability analyses are significantly more computationally efficient, allowing them to be employed effectively for interpretive studies, predictive simulations remain computationally expensive. The high computational cost prevents their routine application in between-shot analysis, where rapid turnaround times are necessary. Addressing these performance limitations will require further optimizations in GPU implementation, potential algorithmic improvements, and the development of hybrid modeling strategies that balance fidelity and efficiency.

5.4 Future Improvements

Making predictive simulations using T3D/GX more feasible demands a set of strategic enhancements through the reduction of computational costs and improving efficiency. Part of this development entails optimization of the GX implementation on the GPU. As GX will be used for nonlinear gyrokinetic turbulent calculation, optimizing performance on GPU architecture is critical. Memory management optimization, kernel performance optimization, and parallelization algorithms can contribute to a great reduction in the time of execution and make high-fidelity turbulence simulation a more feasible option for predictive purposes.

One crucial area of future research is the construction of hybrid models employing reduced physics approximations where necessary. While the most accurate results can be obtained from full gyrokinetic simulations, their computational cost may be so high as to be unaffordable on long timescales for transport. By combining reduced models that capture the key physics but reduce the computational intensity, a compromise between the level of detail and efficiency might be found. These hybrids would make gyrokinetic turbulence modeling feasible in predictive contexts at a reasonable computational cost.

The communication between CPU and GPU elements of TRANSP also has areas for improvement. Optimizing load distribution between the two architectures is essential in precluding bottlenecks and achieving maximum utilization of resources. Optimizing data transfer algorithms and computational workload between CPU transport solvers and GPU turbulent calculations can enhance total efficiency and make it possible for simulations to be scalable and faster.

On top of the optimization of algorithms and hardware, optimizing numerical techniques in TRANSP can also make a difference in computational efficiency. Implementing adaptive time-stepping would enable the time step in the simulation to be varied dynamically according to plasma profile evolution and intensity of the turbulence. This would optimize computational effort by applying finer time resolution only when required while maintaining stability and accuracy throughout the simulation.

Together, these improvements would move TRANSP/T3D/GX calculations closer to practical runtimes for predictive and between-shot applications. By overcoming both the algorithms and the hardware hurdles, future advancements will facilitate better integration of high-accuracy turbulence modeling in everyday plasma transport simulations and improve the predictive capacity of TRANSP

in the long run.

6 Summary and Conclusions

This paper describes two predictive numerical frameworks available in TRANSP. This description complements the earlier paper [3] that documented the TRANSP capabilities, including the predictive solver inputs and initializations, but did not describe the details of the algorithms of PT_SOLVER or provide any verification. The predictive frameworks in TRANSP include the native PT_SOLVER and the recently integrated T3D solver. PT_SOLVER is designed as a parallel, modular, multi-region time-dependent transport solver, and it evolves flux surface average quantities using an implicit Newton-based technique. A set of six coupled equations for density, temperatures of electrons and ions, and toroidal angular momentum is evolved. The integration of transport equations includes various source couplings, geometrical motion terms, a nonlinear convergence constraint, and stabilization mechanisms using modified Péclet numbers to reduce stiffness related to gradient-sensitive closure relations. While T3D also solves coupled 1D equations and uses similar Newton iterations to evolve profiles in a time-dependent fashion, it is geared towards use with high-fidelity gyrokinetic simulations such as those provided by the GX code.

The numerical behavior of the PT_SOLVER is evaluated through a series of hierarchical verification tests, including testing through both analytic and manufactured solutions, performing numerical convergence studies that included coupled equations with stiff gradient-dependent diffusion, and performing code-to-code verification against TGYRO with TGLF and NEO transport models. Overall, these evaluations provide evidence that PT_SOLVER achieves robust nonlinear convergence as well as profile solutions that are consistent with an established reference workflow, so long as equilibrium, sources, and boundary conditions are closely matched. In addition, the multilevel parallelization method, established through adopting the decomposition of computational domains over flux surfaces and providing for a high degree of internal parallelism in the transport model computations, enhances the practical applicability of PT_SOLVER to performing computationally intensive predictive calculations.

This manuscript explains how the interface between TRANSP and the T3D transport solver works. The benchmarks for the T3D and PT_SOLVER provide confirmation that the interface is correct and that the process flow is sound, but not a validation of the models for neoclassical and turbulent transport. As details of the T3D numerical algorithm are discussed elsewhere [21, 22, 32], they will not be repeated here. In the benchmark cases considered here, the coupled interface yields nearly identical profiles when T3D and PT_SOLVER are supplied with the same source terms, impurity constraints, and equilibria. Minor differences arise from the different implementations of the collisional electron-ion exchange terms in PT_SOLVER and T3D.

The T3D/TRANSP interface provides a new framework for predictive analysis with high-fidelity turbulence models and significantly enhances the fidelity of predictive computations in TRANSP. The framework can also be used to port the experiment profiles for linear stability analysis with GX. This additional benefit comes because TRANSP shares the interpretive and predictive workflows within the same framework as described in the TRANSP reference paper [3].

The present work establishes the TRANSP predictive framework as a robust numerical component for predictive modeling and clarifies the present status of modular coupling to external transport and turbulence tools. Future work will focus on broader predictive applications, additional verification of extended transport channels, such as poloidal velocity advances, hybrid reduced and high-fidelity modeling strategies, and further optimization of GPU-enabled turbulence workflows.

Acknowledgments

The research described in this paper was conducted at Princeton Plasma Physics Laboratory, a national laboratory operated by Princeton University for the United States Department of Energy under Prime Contract No. DE-AC02-09CH11466. The United States Government retains a non-exclusive, paid-up, irrevocable, worldwide license to publish or reproduce the published form of this manuscript, or allow others to do so, for United States Government purposes. This research used the resources of the National Energy Research Scientific Computing Center, a DOE Office of Science User Facility supported by the Office of Science of the U.S. Department of Energy under Contract No. DE-AC02-05CH11231.

The authors gratefully acknowledge the late Doug McCune for his leadership, sustained guidance, and encouragement over many years in the development of TRANSP and its predictive capabilities.

Data Availability

Datasets and Python scripts associated with this work are deposited in the Princeton Data Commons (PDC) repository. The repository provides a persistent identifier (DOI) for the deposited materials. The data are released under the Creative Commons Attribution 4.0 International license (CC BY 4.0).¹

Repository landing page: <https://doi.org/10.34770/62xv-ra97>

DOI: 10.34770/62xv-ra97

Users of these datasets should cite (i) this Article and (ii) the corresponding PDC dataset DOI.

References

- [1] R.J. Hawryluk. “An Empirical Approach to Tokamak Transport”. In: *Physics of Plasmas Close to Thermonuclear Conditions*, ed. by B. Coppi, et al. Vol. 1 (1980), pp. 19–46.
- [2] Joshua Breslau et al. *TRANSP*. June 2018. DOI: 10.11578/dc.20180627.4. URL: <https://www.osti.gov/biblio/code-12542>.
- [3] A.Y. Pankin et al. “TRANSP integrated modeling code for interpretive and predictive analysis of tokamak plasmas”. In: *Computer Physics Communications* 312 (2025), p. 109611. ISSN: 0010-4655. DOI: <https://doi.org/10.1016/j.cpc.2025.109611>. URL: <https://www.sciencedirect.com/science/article/pii/S0010465525001134>.
- [4] R.V. Budny. “Alpha heating in ITER L-mode and H-mode plasmas”. In: *Nuclear Fusion* 52.1 (Nov. 2011), p. 013001. DOI: 10.1088/0029-5515/52/1/013001. URL: <https://doi.org/10.1088/0029-5515/52/1/013001>.
- [5] Hyun-Tae Kim et al. “Validation of D–T fusion power prediction capability against 2021 JET D–T experiments”. In: *Nuclear Fusion* 63.11 (Oct. 2023), p. 112004. DOI: 10.1088/1741-4326/ace26d. URL: <https://doi.org/10.1088/1741-4326/ace26d>.
- [6] R. V. Budny and J. G. Cordey. “Core fusion power gain and alpha heating in JET, TFTR, and ITER”. In: *Nuclear Fusion* 56 (2016), p. 056002.
- [7] R. V. Budny and JET Contributors. “Alpha heating, isotopic mass, and fast ion effects in deuterium–tritium experiments”. In: *Nuclear Fusion* 58 (2018), p. 096011.

¹<https://creativecommons.org/licenses/by/4.0/>

- [8] J. Abbate et al. “Large-database cross-verification and validation of tokamak transport models using baselines for comparison”. In: *Physics of Plasmas* 31.4 (2024), p. 042506. DOI: 10.1063/5.0190908.
- [9] G. Avdeeva et al. “Energy transport analysis of NSTX plasmas with the TGLF turbulent and NEO neoclassical transport models”. In: *Nuclear Fusion* 63.12 (Oct. 2023), p. 126020. DOI: 10.1088/1741-4326/acfc56. URL: <https://doi.org/10.1088/1741-4326/acfc56>.
- [10] J. B. Lestz et al. “Assessing time-dependent temperature profile predictions using reduced transport models for high performing NSTX plasmas”. In: *Plasma Physics and Controlled Fusion* 67.10 (2025), p. 105029. DOI: 10.1088/1361-6587/ae0c35.
- [11] J. B. Lestz et al. “Sensitivities of time-dependent temperature profile predictions for NSTX with the Multi-Mode Model”. In: *Plasma Physics and Controlled Fusion* 67.10 (2025), p. 105030. DOI: 10.1088/1361-6587/ae0c34.
- [12] F. Auriemma et al. “TRANSP-TGLF core predictive modeling of the JET DT baseline scenario”. In: *Nuclear Fusion* 66.5 (Apr. 2026), p. 056043. DOI: 10.1088/1741-4326/ae5de2. URL: <https://doi.org/10.1088/1741-4326/ae5de2>.
- [13] G. Pereverzev and P. Yushmanov. *ASTRA automated system for TRansport analysis in a tokamak*. Tech. rep. IPP 5/98. Max-Planck-Institut für Plasmaphysik, 2002.
- [14] G. Cenacchi and A. Taroni. *JETTO: A Free Boundary Plasma Transport Code (Basic Version)*. Tech. rep. JET-IR(88)03. JET / ENEA, 1988.
- [15] M. Romanelli et al. “JINTRAC: A system of codes for integrated simulation of Tokamak scenarios”. In: *Plasma and Fusion Research* 9 (2014), p. 3403023. DOI: 10.1585/pfr.9.3403023.
- [16] J. M. Park et al. “An efficient transport solver for tokamak plasmas”. In: *Computer Physics Communications* 214 (2017), pp. 1–5. DOI: 10.1016/j.cpc.2016.12.018.
- [17] J. M. Park et al. “Integrated modeling of high β_N steady state scenario on DIII-D”. In: *Physics of Plasmas* 25 (2018), p. 012506.
- [18] O. Meneghini et al. “FUSE (Fusion Synthesis Engine): A Next Generation Framework for Integrated Design of Fusion Pilot Plants”. In: *arXiv preprint arXiv:2409.05894* (2024). DOI: 10.48550/arXiv.2409.05894. arXiv: 2409.05894 [physics.plasm-ph].
- [19] Jonathan Citrin et al. “TORAX: A Fast and Differentiable Tokamak Transport Simulator in JAX”. In: *arXiv preprint arXiv:2406.06718* (2024). DOI: 10.48550/arXiv.2406.06718. arXiv: 2406.06718 [physics.plasm-ph].
- [20] S.C. Jardin et al. “On 1D diffusion problems with a gradient-dependent diffusion coefficient”. In: *Journal of Computational Physics* 227.20 (2008), pp. 8769–8775. ISSN: 0021-9991. DOI: <https://doi.org/10.1016/j.jcp.2008.06.032>. URL: <https://www.sciencedirect.com/science/article/pii/S0021999108003616>.
- [21] Tony Qian et al. “Stellarator profile predictions using Trinity3D and GX”. In: *APS Division of Plasma Physics Meeting Abstracts*. Vol. 2022. APS Meeting Abstracts. Jan. 2022, BO03.006.
- [22] Michael Barnes. “TRINITY: A unified treatment of turbulence, transport, and heating in magnetized plasmas”. eprint arXiv:0901.2868. Ph.D. thesis. University of Maryland, 2008. arXiv: 0901.2868 [physics.plasm-ph].
- [23] N. R. Mandell, W. Dorland, and M. Landreman. “Laguerre-Hermite pseudo-spectral velocity formulation of gyrokinetics”. In: *Journal of Plasma Physics* 84.1 (2018), p. 905840108. DOI: 10.1017/S0022377818000041.

- [24] N. R. Mandell et al. “GX: a GPU-native gyrokinetic turbulence code for tokamak and stellarator design”. In: *Journal of Plasma Physics* 90.4 (2024), p. 905900402. DOI: 10.1017/S0022377824000631.
- [25] S. C. Jardin, N. Pomphrey, and J. DeLucia. “Dynamic modeling of transport and positional control of tokamaks”. In: *Journal of Computational Physics* 66.2 (1986), pp. 481–507. DOI: 10.1016/0021-9991(86)90077-X.
- [26] Stephen Jardin. *Computational Methods in Plasma Physics*. Boca Raton: CRC Press, 2010. ISBN: 9780429075537. DOI: 10.1201/EBK1439810958. URL: <https://www.taylorfrancis.com/books/mono/10.1201/EBK1439810958/computational-methods-plasma-physics-stephen-jardin>.
- [27] G.V. Pereverzev and G. Corrigan. “Stable numeric scheme for diffusion equation with a stiff transport”. In: *Computer Physics Communications* 179.8 (2008), pp. 579–585. ISSN: 0010-4655. DOI: 10.1016/j.cpc.2008.05.006. URL: <https://www.sciencedirect.com/science/article/pii/S001046550800218X>.
- [28] Andrei Ludvig-Osipov, Dmytro Yadykin, and Pär Strand. “High-order implicit solver in conservative formulation for tokamak plasma transport equations”. In: *Computer Physics Communications* 311 (2025), p. 109570. DOI: 10.1016/j.cpc.2025.109570.
- [29] Federico Felici et al. “Real-time-capable prediction of temperature and density profiles in a tokamak using RAPTOR and a first-principle-based transport model”. In: *Nuclear Fusion* 58.9 (2018), p. 096006. DOI: 10.1088/1741-4326/aac8f0.
- [30] Simon Van Mulders et al. “Rapid optimization of stationary tokamak plasmas in RAPTOR: demonstration for the ITER hybrid scenario with neural network surrogate transport model QLKNN”. In: *Nuclear Fusion* 61.8 (2021), p. 086019. DOI: 10.1088/1741-4326/ac0d12.
- [31] J. Candy et al. “Tokamak profile prediction using direct gyrokinetic and neoclassical simulation”. In: *Physics of Plasmas* 16.6 (2009), p. 060704. DOI: 10.1063/1.3167820.
- [32] M. Barnes et al. “Direct multiscale coupling of a transport code to gyrokinetic turbulence codes”. In: *Physics of Plasmas* 17.5 (2010), p. 056109. DOI: 10.1063/1.3323082.
- [33] R. E. Waltz et al. “A gyro-Landau-fluid transport model”. In: *Physics of Plasmas* 4.7 (1997), pp. 2482–2496. DOI: 10.1063/1.872228. URL: <https://doi.org/10.1063/1.872228>.
- [34] Jonathan E. Kinsey, Gary M. Staebler, and Ronald E. Waltz. “Burning Plasma Confinement Projections and Renormalization of the GLF23 Drift-Wave Transport Model”. In: *Fusion Science and Technology* 44.4 (2003), pp. 763–775. DOI: 10.13182/FST03-A414. URL: <https://doi.org/10.13182/FST03-A414>.
- [35] J. E. Kinsey, G. M. Staebler, and R. E. Waltz. “The first transport code simulations using the trapped gyro-Landau-fluid model”. In: *Physics of Plasmas* 15.5 (2008), p. 055908. DOI: 10.1063/1.2889008.
- [36] G. M. Staebler, J. E. Kinsey, and R. E. Waltz. “Gyro-Landau fluid equations for trapped and passing particles”. In: *Phys. Plasmas* 12 (2005), p. 102508. DOI: 10.1063/1.2044587.
- [37] T. Rafiq et al. “Physics basis of Multi-Mode anomalous transport module”. In: *Physics of Plasmas* 20.3 (2013), p. 032506. DOI: 10.1063/1.4794288.
- [38] T. Rafiq et al. “Microtearing modes in tokamak discharges”. In: *Physics of Plasmas* 23.6 (2016), p. 062507. DOI: 10.1063/1.4953609.

- [39] P-H. Rebut, P.P. Lallia, and M.L. Watkins. “The critical temperature gradient model of plasma transport: Applications to JET and future tokamaks”. In: *Plasma Physics and Controlled Nuclear Fusion Research (Proc. 12th IAEA Conf., Nice, France)*. Vol. 2. IAEA, 1989, p. 191.
- [40] S.C. Jardin, M.G. Bell, and N. Pomphrey. “TSC simulation of Ohmic discharges in TFTR”. In: *Nuclear Fusion* 33.3 (Mar. 1993), p. 371. DOI: 10.1088/0029-5515/33/3/I01. URL: <https://dx.doi.org/10.1088/0029-5515/33/3/I01>.
- [41] A Fukuyama et al. “Transport simulation on L-mode and improved confinement associated with current profile modification”. In: *Plasma Physics and Controlled Fusion* 37.6 (June 1995), p. 611. DOI: 10.1088/0741-3335/37/6/002. URL: <https://dx.doi.org/10.1088/0741-3335/37/6/002>.
- [42] N Takei et al. “Intermittent β collapse after NBCD turn-off in JT-60U fully non-inductive reversed shear discharges”. In: *Plasma Physics and Controlled Fusion* 49.3 (Feb. 2007), p. 335. DOI: 10.1088/0741-3335/49/3/011. URL: <https://dx.doi.org/10.1088/0741-3335/49/3/011>.
- [43] J.D. Callen. “Paleoclassical electron heat transport”. In: *Nuclear Fusion* 45.9 (Aug. 2005), p. 1120. DOI: 10.1088/0029-5515/45/9/012. URL: <https://dx.doi.org/10.1088/0029-5515/45/9/012>.
- [44] C. S. Chang and F. L. Hinton. “Effect of impurity particles on the finite-aspect ratio neoclassical ion thermal conductivity in a tokamak”. In: *The Physics of Fluids* 29.10 (Oct. 1986), pp. 3314–3316. ISSN: 0031-9171. DOI: 10.1063/1.865847. eprint: https://pubs.aip.org/aip/pfl/article-pdf/29/10/3314/12413384/3314_1_online.pdf. URL: <https://doi.org/10.1063/1.865847>.
- [45] E A Belli and J Candy. “Kinetic calculation of neoclassical transport including self-consistent electron and impurity dynamics”. In: *Plasma Physics and Controlled Fusion* 50.9 (July 2008), p. 095010. DOI: 10.1088/0741-3335/50/9/095010. URL: <https://dx.doi.org/10.1088/0741-3335/50/9/095010>.
- [46] E A Belli and J Candy. “Full linearized Fokker–Planck collisions in neoclassical transport simulations”. In: *Plasma Physics and Controlled Fusion* 54.1 (Dec. 2011), p. 015015. DOI: 10.1088/0741-3335/54/1/015015. URL: <https://dx.doi.org/10.1088/0741-3335/54/1/015015>.
- [47] W. A. Houlberg et al. “Bootstrap current and neoclassical transport in tokamaks of arbitrary collisionality and aspect ratio”. In: *Physics of Plasmas* 4.9 (Sept. 1997), pp. 3230–3242. ISSN: 1070-664X. DOI: 10.1063/1.872465. eprint: https://pubs.aip.org/aip/pop/article-pdf/4/9/3230/19108363/3230_1_online.pdf. URL: <https://doi.org/10.1063/1.872465>.
- [48] H.G. Dudding et al. “A new quasilinear saturation rule for tokamak turbulence with application to the isotope scaling of transport”. In: *Nuclear Fusion* 62.9 (July 2022), p. 096005. DOI: 10.1088/1741-4326/ac7a4d. URL: <https://doi.org/10.1088/1741-4326/ac7a4d>.
- [49] Tom F. Neiser et al. “Database generation for validation of TGLF and retraining of neural network accelerated TGLF-NN”. In: *APS Division of Plasma Physics Meeting Abstracts*. Abstract GP11.00010. 2022, GP11.00010.
- [50] Tom F. Neiser et al. “Multi-fidelity neural network representation of gyrokinetic turbulence”. In: *APS Division of Plasma Physics Meeting Abstracts*. Abstract PP11.00039. 2023, PP11.00039.

- [51] G. M. Staebler, J. E. Kinsey, and R. E. Waltz. “Gyro-Landau fluid equations for trapped and passing particles”. In: *Physics of Plasmas* 12.10 (2005), p. 102508. DOI: 10.1063/1.2044587.
- [52] G. M. Staebler, J. E. Kinsey, and R. E. Waltz. “A theory-based transport model with comprehensive physics”. In: *Physics of Plasmas* 14.5 (2007), p. 055909. DOI: 10.1063/1.2436852.
- [53] Emily Ann Belli and Jeff Candy. “Kinetic calculation of neoclassical transport including self-consistent electron and impurity dynamics”. In: *Plasma Physics and Controlled Fusion* 50 (2008), p. 095010.
- [54] T.F. Neiser. “Large Database Validation of TGLF on DIII-D and MAST-U Plasmas”. In: *US-EU Transport Task Force*. Asheville, NC, Apr. 2024. URL: <https://conferences.union.wisc.edu/ttf/conference-agenda/>.
- [55] M. Giacomini et al. “A quasi-linear model of electromagnetic turbulent transport and its application to flux-driven transport predictions for STEP”. In: *Journal of Plasma Physics* 91.1 (2025), E16. DOI: 10.1017/S0022377824001107.
- [56] Princeton Plasma Physics Laboratory. *Guide to Running TRANSP/T3D/GX Coupled Simulations*. TRANSP documentation page. 2026. URL: <https://transp.pppl.gov/modules/t3d.html>.